Chapter 1

Intracorporeal Millirobotics

1.1. Introduction

Intracorporeal millirobots are at the boundary of conventional surgical robots that are installed in the operating room (OR) along the table or on the patient. They still work in the macroworld, where volumic forces and torques (such as weight) dominate. Under this designation, we mean devices with either partially or fully intracorporeal actuated degrees of freedom (DoFs). Their dimensions in the body can reach at the maximum a few tens of millimeters. The dimensions of the surgical site range from a few millimeters to a few centimeters; however, when it is mobile, the millirobot may cover a workspace of several cubic centimeters. The forces exerted on tissues by the robot range from a few millinewtons to several newtons, up to tens of newtons for retraction of organs or gripping a needle.

At this scale, many prototypes have been developed, even though very few of them have entered the OR. In many cases, they look like conventional robots for which rigid body kinematic models and vision-based or force-based control algorithms may be used. More or less, they could be seen as miniaturized versions of existing solutions.

However, to comply with the environment constraints (biological tissues, safety, etc.) and the task constraints (access to deep anatomical spaces, preservation of vital structures, high dexterity, etc.), many efforts have been made to design original kinematics with advanced sensing capabilities for manipulation and locomotion purposes. A promising approach is now to integrate robotics in instruments rather than to think of the robot as a simple instrument holder.

In section 1.2, we will present a variety of millimetric devices providing intracorporeal manipulation and/or mobility capabilities. In section 1.3, we will address scientific issues that are specific to robotics at milliscale. These issues cover the main fields of robotic research in modeling, design, actuation, sensing and control. In section 1.4, we will present in more detail three robotic systems that are representative of the state of the art at the milliscale: a dual-arm master–slave system, a snake-like robot made up of concentric tubes and a handheld robotized instrument.

1.2. Principles

We present in this section the principles of three classes of devices:

– partially intracorporeal devices with active distal mobilities;

– intracorporeal manipulators;

– intracorporeal mobile devices.

Their purpose is functional exploration (in the case of capsules) as well as intervention (to remove a polyp, place a stent, deliver a drug in a localized manner, etc., but also cut, retract, dissect and cauterize as in conventional surgery). Emphasis has been put on several representative devices of each class to review functional qualities and limits of potential robotic solutions. A more comprehensive review of many prototypes worldwide can be found in [DOM 12b].

1.2.1. *Partially intracorporeal devices with active distal mobilities*

Under this denomination, we mean conventional instruments that have been modified to improve dexterity and/or precision of the surgeon or the radiologist. We include, for instance, any device providing two additional actuated DoFs between the entry port in the body and the tool (retractor, forceps, needle driver, but also tip of an endoscope), not accounting for the closing/opening of the jaws of the tool if any. The partially intracorporeal device is generally attached to an external device that can be a robot providing supplementary DoFs. It is driven externally by the surgeon, either directly in a comanipulation mode (section 1.3.5.3) or from a master workstation in a teleoperation mode (section 1.3.5.2) (Figure 1.1).

With such a definition, we consider entering into this class the actuated instruments for endoscopic surgery and the catheters. Typically, the diameter of these instruments is restricted to 8–10 mm in abdominal surgery, 5–6 mm in cardiac surgery, even 2.5–3 mm for intrauterine fetal surgery [HAR 05, ZHA 09a], 0.5–2 mm for an active catheter.

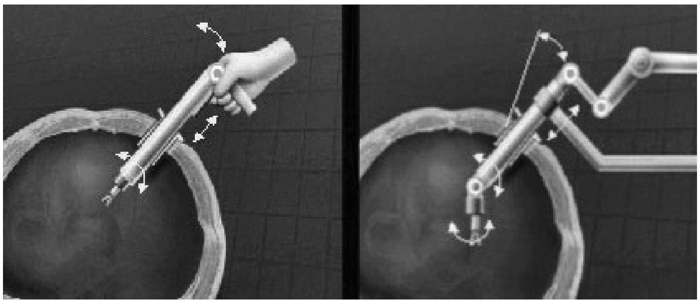

a) b)

Figure 1.1. *Partially intracorporeal DoFs: a) comanipulated instrument; b) teleoperated instrument [SAL 04]*

1.2.1.1. *Actuated instruments for endoscopic surgery*

As opposed to open surgery, endoscopic surgery has revolutionized surgical practice since the early 1970s. Often referred to as minimally invasive surgery (MIS), it reduces postsurgery wounds, the risk of infection, the recovery time and the cost of treatment. But it suffers from a certain number of shortcomings: loss of internal mobility due to kinematic constraints induced by the trocar, hand–eye coordination due to the inversion of directions of motion of the hands and the tool tip, loss of force and tactile feedback, restricted workspace and surgeon's fatigue. These limitations have motivated the development and introduction of robots in the OR. Since the mid-1990s, with the robotic systems ZEUS (Computer Motion[1]) and Da Vinci (Intuitive Surgical[2]), master–slave architecture has been adopted for MIS: the instruments are carried by two or three slave manipulators teleoperated by the surgeon from a remote master console. Along the same lines, it is worth mentioning the platforms Raven II from University of Washington [HAN 13] and MiroSurge from DLR [HAG 10] that are dedicated to research in robotic surgery.

1 Merged with Intuitive Surgical since 2003.

2 http://www.intuitivesurgical.com/.

In these systems, the active part of each instrument may have up to two actuated DoFs (not including actuation of the gripper) mounted at the distal end of a rigid hollow tube through which the driving cables pass (Figure 1.2, left). Such additional DoFs may also be mounted at the distal part of a lightweight handheld system (Figure 1.2, right) that gives the surgeon the ability to comanipulate the instrument without using a master arm [ZAH 10]. In both cases, the additional pan and tilt rotations compensate for the loss of mobility induced by the constraint of passage through the trocar.

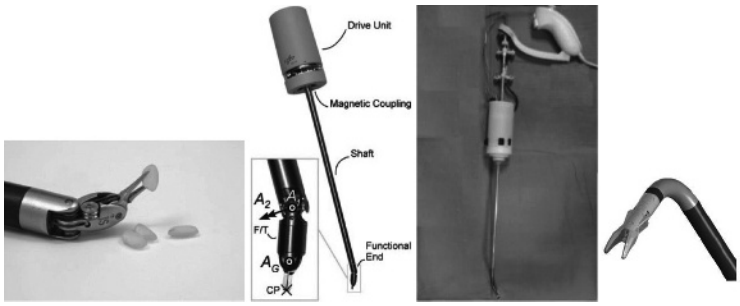

Figure 1.2. *From left to right: close-up of the Da Vinci Endowrist tip manipulating rice grains; DLR MICA instrument of the MIRO platform for endoscopic surgery and close-up of the two-DoF wrist mounted with a force/torque (FT) sensor [HAG 10]; the EndoControl[3] handheld laparoscopic instrument JAiMY [ZAH 10]; close-up of the two-DoF bending and rotary wrist of JAiMY*

1.2.1.2. *Actuated catheters*

A catheter is a thin (a few millimeter in diameter), long (of the order of a meter) and hollow tube that allows the passage of functional catheters of smaller diameter. These may hold various miniature sensors (pressure, ultrasound probe, optical fiber, etc.) or instruments, e.g. for the local administration of a drug, the insertion of a prosthesis (stent, angioplasty balloon, etc.), the endovascular coiling of aneurysms, the puncture/biopsy for diagnostic purposes or tumor destruction (radiofrequency abalation, laser therapy, etc.) [CHA 00]. The catheter is inserted into an artery, usually in the groin. It is steered, under radiographic control, by the doctor who rotates it around its longitudinal axis and pushes it to its destination. This is made difficult because of the narrowness of the vessel, the frictions on the wall and the many bifurcations. The difficulty for the surgeon is thus to transmit force and motion to the end effector with little or no relevant kinesthetic feedback,

3 http://www.endocontrol-medical.com/.

and with a restricted and sparse visual feedback to limit the radiation doses, while avoiding perforation of the artery.

An active catheter is shown in Figure 1.3 [SZE 11]. It is endowed with guidance abilities to facilitate its introduction in bifurcations that exhibit restrictive directions (including very acute closed angles). There are some similarities between an active catheter and a teleoperated robotized colonoscope, however, the diameter is nearly one order of magnitude lower, typically 1–2 mm (the diameter can be reduced to 0.5–1 mm in the case of a guidance catheter). The other difference, and the major difficulty, is that the catheter must move in an artery where the pressure and the blood flow are important. Many prototypes of active catheters have been developed over the last 10 years where many actuation concepts have been explored as will be presented in section 1.3.3.

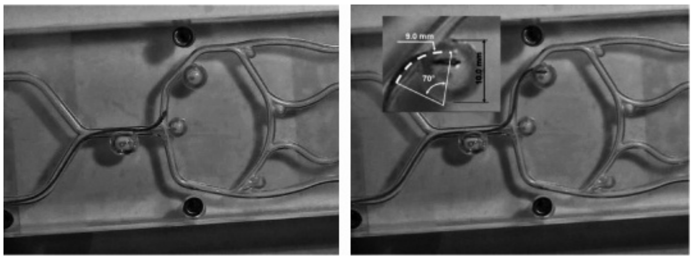

Figure 1.3. *Navigation of an active catheter in a phantom of an aneurysm in the Willis Polygon (Ø = 1.1 mm, radius of curvature = 9 mm) [SZE 11]*

To protect the surgeon against radiation, master–slave systems, which allow the doctor to remotely control the catheter, are now available, such as the Sensei X Robotic System, and more recently the Magellan Robotic System, both marketed by Hansen Medical[4], or the Amigo RSC from Catheter Robotics[5]. These systems offer a steering unit that pushes and allows bidirectional rotations of the catheter tip.

1.2.2. *Intracorporeal manipulators*

We give the name intracorporeal manipulators to any device providing full (or at least more than 2) mobility to the tool with actuated DoFs located

4 http://www.hansenmedical.com/.
5 www.catheterrobotics.com/rcs-main.htm.

between the entry port in the body and the tool. These devices may be minimanipulators (scaled version of conventional robot arms) or flexible instruments designed to perform new techniques of surgery without visible scaring. We also include in this class modular approaches aiming at assembling and disassembling (or possibly deploying and retracting) robots and platforms within the body.

1.2.2.1. *Minimanipulators*

Typically, minimanipulators have a centimetric size, generating submillimetric to centimetric displacements and can exert forces of the order from 1 N (e.g. to insert a needle into a coronary artery) to several tens of newtons to retract tissue. Different options may be adopted in the design:

– discrete architectures with embedded actuators;

– discrete architectures with remote actuators (outside the patient);

– continuum architectures (or snake-like or elephant trunk like architectures) with remote actuators.

Discrete architectures have a limited number of rigid links and discrete joints. A first example of such robot with embedded actuators, designed for *natural orifice transluminal endoscopic surgery* (NOTES) (section 1.2.2.2), is shown in Figure 1.4 [LEH 08, TIW 10]: it consists of two prismatic arms each connected to a central body by a revolute joint, together providing four planar DoFs. Each arm is fitted with either a grasper forceps or a cautery end effector. The central body contains a stereo camera pair and magnets that interact with external magnets to attach the robot to the interior abdominal wall. It is inserted through the esophagus and into the peritoneal cavity using an overtube in a configuration where the arms are disconnected from the central body.

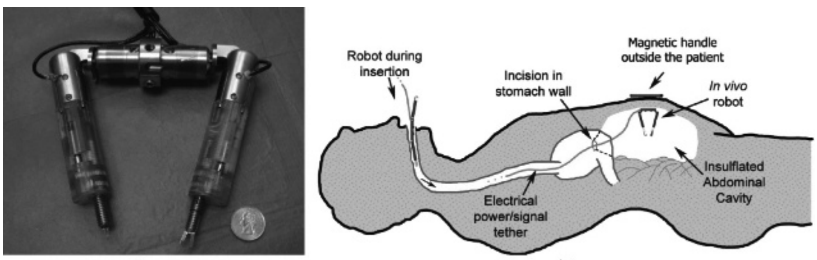

a) b)

Figure 1.4. *a) In vivo two-arm dexterous robot from Vanderbilt University; b) NOTES procedure [LEH 08, TIW 10]*

Another example is the modular robot DRIMIS [SAL 04] (Figure 1.5(a)), which is the result of an optimization procedure using multiobjective evolutionary algorithms, coupled with a realistic simulation of the intended surgical task (anastomosis during coronary artery bypass grafting). Several one-DoF and two-DoF modules (Ø 10 mm, 25–40 mm long) were designed with different axis organization. Typically, a six-DoF arm is 120 mm long.

The arms of the dual-arm robot SPRINT have a similar kinematics. The platform was developed in the frame of the EU FP7 Araknes project[6] [PIC 10, SAN 11] (Figure 1.5(b)). Each arm has six DoFs plus the gripper. Four additional DoFs are provided by the external positioning device. In its current version, the size is 18 mm in diameter and 120 mm in length. It can exert forces up to 5 N. The robot is intended to be attached to the umbilical access port in *single-port access* (SPA) surgery (see section 1.2.2.2). A detailed description of the system is presented in section 1.4.1.

a) b)

Figure 1.5. *Architectures with rigid links and discrete joints: a) DRIMIS (ISIR) [SAL 04]; b) SPRINT (Araknes project) [PIC 10, SAN 11]*

When miniature actuators are embedded in the structure, one of the difficulties is the routing of the electrical cables, another is the small power-to-weight ratio of the actuators available at this size, dramatically restricting the forces that can be exerted by the robot on tissues. The latter no longer holds with remote actuators. However, remote actuation implies using mechanical wires to drive the joint, which is a more tricky issue than routing electrical cables. An example of such an architecture designed by Ikuta *et al.* [IKU 03] is depicted in Figure 1.6: the Hyper Finger (Mark-3) is a seven-DoF (including the forceps griping action) wire-driven active forceps for laparoscopic surgery (Ø 10 mm). A special decoupled two-DoF “ring-joint”

6 http://www.araknes.org/home.html.

mechanism was developed, where each DoF can be driven independently. It is teleoperated with an analogous seven-DoF master finger.

An interesting alternative to the discrete aforementioned minimanipulators is the continuum robots. They have a smaller outer diameter with comparable performance specifications [XU 12]. They more or less extend the design used for bending the tip of active catheters. The actuators are placed outside the patient, pulling cables or “tendons” of different technologies to control distributed stiffness and curvature, as will be discussed in section 1.3.3. Zhang *et al.* [ZHA 11] have designed a six-DoF wire-driven robotic manipulator for fetal surgery, namely to place a detachable silicone balloon in the fetal trachea for treatment of congenital diaphragmatic hernias. The robot is constituted of three units, each having two DoFs. The size is 2.4 mm in diameter. The contact force of the robot is controlled to be less than 0.3 N.

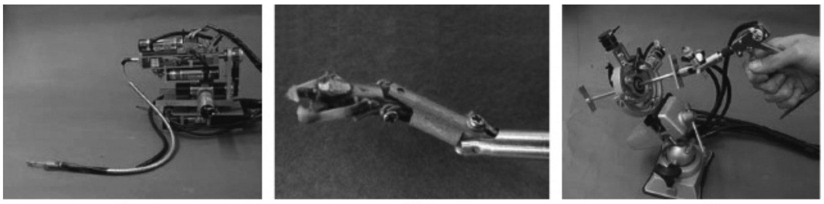

a) b) c)

Figure 1.6. *Hyper Finger [IKU 03]: a) seven-DoF slave manipulator at the end of a guide tube; b) close-up of the seven-DoF manipulator; c) master manipulator*

To navigate in a constrained operating workspace, circumventing vital organs and risky areas, a higher number of DoFs is required. HARP (highly articulated robotic probe) is a continuum and hyper-redundant robot proposed by [DEG 06, OTA 08] for pericardial interventions. It is made up of two snake-like concentric tubes (Figure 1.7) that can maintain the three-dimensional (3D) shape of the path they follow: each snake can be rigid or limp, and HARP progresses forward by alternating the rigidity/limpness of both snakes. Each snake consists of 50 rigid cylindrical links articulated by spherical joints (±15° in both directions) and strung together by cables (four for HARP). It is 12 mm in diameter, 300 mm in length and can achieve a 75 mm radius of curvature (reduced to 35 mm in a later version). The flexibility of each tube varies according to the tension of the cables. This technological approach is now integrated into the robot-assisted platform of Medrobotics[7].

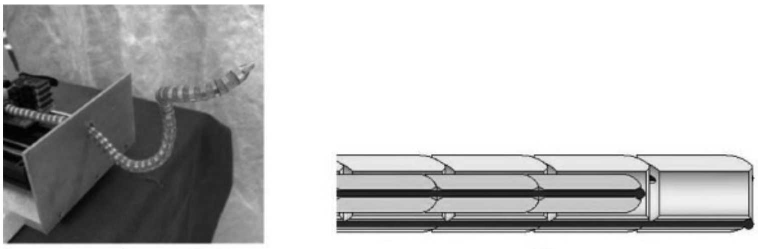

a) b)

Figure 1.7. *Continuum architecture: a) HARP [OTA 08]; b) side cross-sectional view of the two concentric snakes [DEG 06]*

An interesting concept, proposed by Dupont [SEA 06] and Webster [WEB 06a], consists of several pre-bent concentric hollow tubes made up of a super-elastic material such as Nitinol (Nickel Titanium alloy also referred to as NiTi). The resulting snake-like robot (Figure 1.8) may deform continuously by independently translating and/or rotating each tube with respect to the tube in which it is inserted. It has several advantages: it is lightweight; it can be customized in diameter and length to meet the requirements of the operation at hand; it has a very good dexterity and can be deployed while avoiding vital structures; knowing its stiffness makes it possible to evaluate the interaction forces with tissues. We will discuss more in detail design and modeling issues associated with such a robot in section 1.4.2.

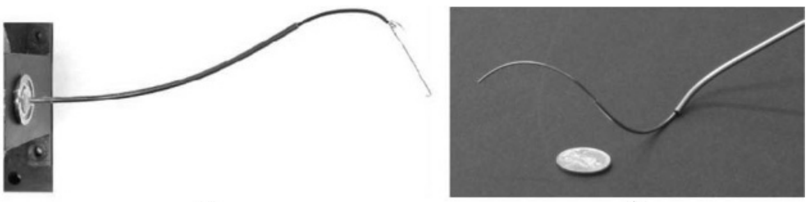

a) b)

Figure 1.8. *a) Prototype of a miniature concentric tube robot of Boston University grasping a needle [SEA 06];b) prototype of JHU [WEB 06a]*

7 http://www.cardiorobotics.com/.

1.2.2.2. *NOTES and SPA devices*

Two new paradigms of surgery are currently being developed within the field of MIS: the transluminal surgery, also known as NOTES [JAG 05, PAR 05], and the surgery through single trocar or single incision [PIS 99, DAL 02], also known as SPA surgery. The common point of these techniques is the absence of new visible scarring as the entry port for the instruments is the mouth, the nose, the anus, the vagina or the urethra for NOTES, or the umbilicus (that can be seen as a cicatrized natural orifice) for SPA. NOTES and SPA are intended to further reduce postoperative complications compared to traditional laparoscopic MIS. This is not yet in common clinical practice, even if hundreds of operations have been performed in preclinic tests on humans worldwide (cholecystectomies, appendectomies, tubal ligations, hysterectomies, gastric sutures, colic sutures, etc.) [MAR 07a, SWA 07].

For NOTES, the technique relies on the use of cable-driven flexible endoscopes with flexible instruments passing through service channels, with which the surgeon can reach and operate the targeted internal organ. Dedicated prototypes have been developed, with additional DoFs to provide enough mobility to the instruments as the examples in Figure 1.9 depict. However, the manipulation is difficult and non-intuitive for a surgeon alone due to the high number of DoFs and the flexibility. One solution is to require the assistance of a second surgeon, another is to robotize the flexible endoscope such that it can be operated by one surgeon from a master robot. As underlined in [TIW 10], robotics may provide better visualization, precision and maneuverability in large cavities, fine motor control of endoscope distal tip and enhanced surgical dexterity.

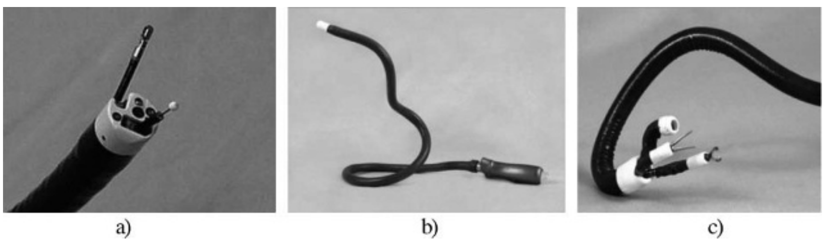

Figure 1.9. *Manual flexible endoscopes for NOTES: a) tip of the R-Scope from Olympus Optical; b) Cobra from USGI Medical: the flexible sheath is rigidly lockable at any time in a desired configuration; c) close-up of the tip of Cobra*

An example of a robotized endoscope for gastrointestinal (GI) procedures is shown in Figure 1.10(a). It shows the 3D model of a two-arm manipulator attached to a flexible endoscope [LOW 06], each arm having five DoFs, not accounting for the opening/closing of the end effector. Tendon-sheath actuation is used. The arms are teleoperated from a master system. The size of the whole manipulator is approximately 25 mm in diameter. Compared with conventional colonoscopes with working channels through which a tool can be inserted, for instance, to cut a polyp, such manipulator may serve to perform more dexterous actions such as suturing.

Another concept was implemented in the prototype of the Anubis project [BAR 12] as shown in Figure 1.10(b). It consists of a flexible endoscope (from Karl Storz Endoskope GmbH) and two flexible hollow arms. Each of these three parts is made up of a long flexible passive shaft and an articulated distal tip. The hollow arms are fixed on the circumference of the main endoscope at the end part of its bending tip. This is done due to a special end cap that deflects the arms from the main direction of the endoscope to provide triangulation between the arms and the endoscope. The distal tip of each arm provides two DoFs to which the translation and rotation of the instrument inside the arm should be added.

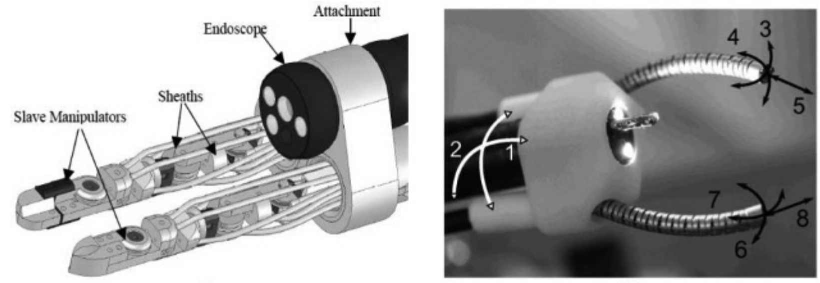

a) b)

Figure 1.10. *Robotized endoscope for NOTES: a) a two-arm manipulator attached to a flexible endoscope from Nanyang University, Singapore [LOW 06]; b) head of the prototype of Anubis project [BAR 12]*

Several technical and scientific issues are still open and research works are underway in many places to extend this endoluminal approach to more demanding therapeutic procedures. To list a few, progress is required in the design to transmit enough forces for performing the desired task, to improve triangulation for better visualization, etc., while continuing miniaturization. Progress is also required in control to better stabilize the surgical tools once on the operating site, to compensate for flexibilities, backlashes, dead-bands, etc., in order to improve precision and dynamics.

Concerning SPA, the challenge is in the design of the trocar and instruments going through it, such that they are deployed inside the abdominal cavity in an optimal working configuration. In other words, they should not collide with each other while offering sufficient triangulation to provide enough dexterity and field of view. A few products for manual procedures are now on the shelves such as, for instance, the ASC Triport and Quad-port[8] or the X-Cone from Karl Storz[9] (see, for instance, [NET 09] for a survey of the techniques and devices or more recently the slides of R. Brandina[10]). Intuitive Surgical has also developed a 5-lumen port[11] for SPA surgery with dedicated curved instruments to go with it (incision of Ø 20–25 mm).

Several ongoing projects aim at robotizing the instruments in order to provide teleoperation functionalities to the surgeon. For instance, the insertable robotic effectors platform (IREP) [BAJ 12] (Figure 1.11(a)) is composed of two seven-DoF continuum arms (not accounting for the grippers' action), each equipped with a one-DoF rotary wrist, two two-DoF continuum segments and a two-DoF planar translational module. It is completed with a three-DoF stereo vision module. It requires only a 15 mm diameter incision.

The ViaCath (Figure 1.11(b)) made use of many components developed originally for the Laprotek, the former robotic system for laparoscopy of EndoVia Medical. It has also seven DoFs, consisting of a rotary wrist and two continuum segments as well, but here a segment has two-DoF bending motion and a third DoF varying length by compression. Moreover, the segments do not have the same length (10 mm and 25 mm, respectively) to optimize the range of motion and force capabilities (0.5 N of lateral force). Figure 1.11(c) shows two ViaCaths and an endoscope surrounded in a Ø 19 mm overtube [ABB 07].

---

8 http://www.advancedsurgical.ie/.

9 https://www.karlstorz.com/cps/rde/xchg/SID-418D6111-3FA54782/karlstorz-en/hs.xsl/8880.htm.

10 http://fr.slideshare.net/urovideo/single-port-technologies.

11 http://www.intuitivesurgical.com/products/davinci_surgical_system/da-vinci-single-site/.

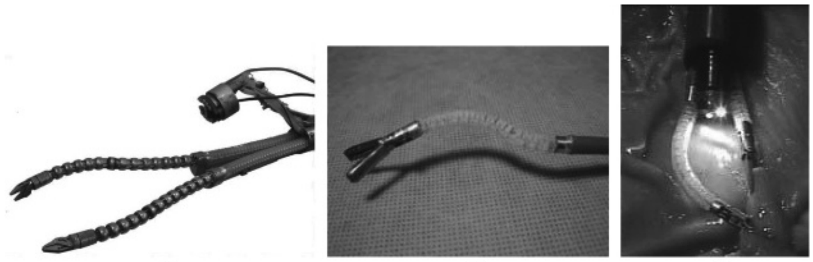

a) b) c)

Figure 1.11. *Robotized instruments for SPA: a) IREP from Vanderbilt and Columbia Universities [BAJ 12]; b) the ViaCath instrument c) in a dual-arm configuration [ABB 07]*

Another seven-DoF arm, again with a rotary wrist but with three two-DoF continuum segments, can be found in [XU 09]. Xu and Zheng [XU 12] have shown that a structure consisting of two segments with a varying length, such as the ViaCath, generates the best distal dexterity when compared to a structure with a translational module, such as the IREP, or a structure with three segments. In their work, the distal dexterity is defined as the solid angle swept by the axis of the arm's gripper at selected points in the robot workspace. For them, such a structure would not only generate a larger workspace but would also allow surgeons to better orient tools as desired.

1.2.2.3. *Modular robots and platforms*

To minimize further the invasiveness of operations, it is necessary to make use of more complex instruments, which are necessarily more bulky, or to realize gestures that simultaneously involve several instruments. It can be envisioned to introduce them as spare parts of the trocar and then to proceed to an intracorporeal assembly. At the end of the procedure, the system is disassembled and taken out: in [OHS 08], an assemblable three-fingered five-DoF hand (Ø 5–6 mm, length 61–67 mm depending on the finger) was designed to handle (push, lift, dislocate, etc.) the organs in the abdominal cavity (Figures 1.12(a) and (b)).

Another solution is to introduce deployable instruments, for instance, in [OLE 05] a camera mounted on a pan-tilt turret (Ø 15 mm) equipped with stabilization legs folded during the passage through the trocar. It is simply deposited in the abdominal cavity, providing the surgeon with a global view of the operative field that advantageously supplements the standard endoscopic vision. More complicated is the skillful detachable-fingered hand described in [TAK 07] to retract organs during laparoscopic surgery (Figure 1.12(c)). It aims at replacing one of the surgeon's hands during hands-assisted laparoscopic surgery (HALS), a technique indicated in complex procedures when the conventional laparoscopic instruments cannot do the work. The three fingers are inserted through a trocar and mounted on a rod inside the abdominal cavity. Therefore, the size of the trocar constrains the diameters of the fingers and of the rod (respectively Ø 8 mm and Ø 12 mm for the version where the fingers are independently driven). The fingers must be easily assembled and disassembled without exerting excessive force in the abdominal cavity.

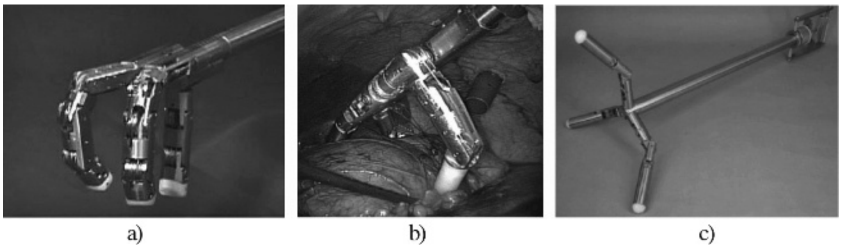

Figure 1.12. *Modular robots: a and b) three-fingered five-DoF assemblable hand [OHS 08]; c) detachable-fingered hand to retract organs during HALS [TAK 07]*

A yet more complicated concept is the modular robot designed for the exploration of the GI tract discussed in [HAR 09]. The modules are swallowable and assembled in the stomach cavity (Figure 1.13(a)). The resulting robot is self-reconfigurable to meet the size constraints that it comes across and the tasks it has to perform. A two-DoF structural module was prototyped (Figure 1.13(b)), containing a battery, two brushless motors and a dedicated control board embedding wireless functionalities. The module size (Ø 15.4 mm, length 36.5 mm) should still be miniaturized. Two permanent magnets are attached at each end of the module for self-aligning and docking purposes. A biopsy module has also been developed with compatible components to fit the structural modules. Derived from this concept, the primary goal of the Araknes project was to introduce into the stomach, via the esophagus, centimeter-sized robots (Figure 1.13(c)), each with a very specific function, and to organize them into a network so that they cooperate to achieve common tasks in bariatric surgery (gastroesophageal reflux, stomach stapling, etc.).

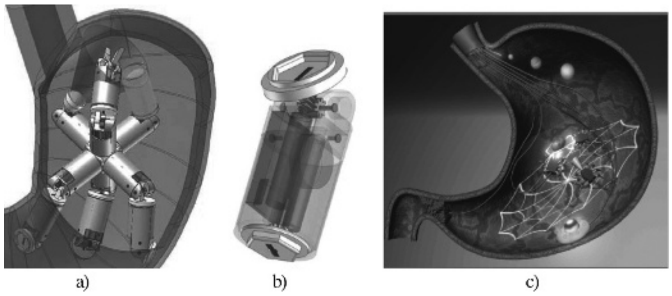

Figure 1.13. *Modular platforms: a) artist view of the assembly in the stomach from elementary modules of a reconfigurable platform and b) CAD drawing of a structural module [HAR 09]; ARAKNES project: c) artist' view of the deployment in the stomach of a network of minirobots*

Nagy *et al.* [NAG 07, NAG 08] went further toward miniaturization, also using small permanent magnets as the driving mechanism of self-assembling modules. A magnetic self-aligning hermaphroditic (MASH) connector has been designed: a small magnetic dipole (typically $3 \times 3 \times 1$ mm^3) is glued on each mating face of a module and oriented perpendicular to the connection axis as shown in Figure 1.14(a). It allows a robust and deterministic connection between modules facilitating the implementation of an intramodule communication bus. The MASH connector, associated with a long-range interaction model predicting higher attractive forces, has proven its efficiency, successfully achieving self-assembly of free-floating objects. An example of a snake-type robot is shown in Figure 1.14(b). The modules have a cylindrical shape (Ø 9 mm) with length 7 mm or 14 mm. Small cylindrical magnets (Ø 4 mm, length 10 mm) may be placed between the modules providing a one-DoF rotary joint, thus allowing the robot to adapt itself to the GI tract. The modules may be docked in commercially available pharmaceutical capsules, used as carriers for ingestion.

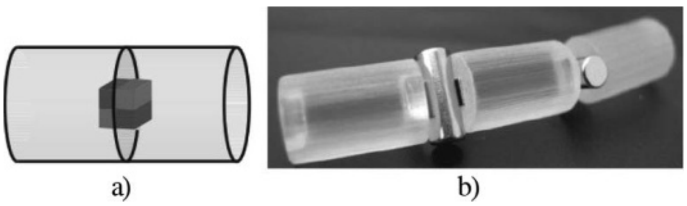

Figure 1.14. *a) Two modules connected by MASH connectors; b) self-assembled two-DoF snake-type modular robot [NAG 07, NAG 08]. Note the two cylindrical magnets between the modules acting as rotary joints*

The underlying scientific and technological challenges to design modular robotic systems are manifold: design of the instruments, sensors, miniaturization and integration of modules, wireless communication between the modules and with the master system, energy autonomy, control and monitoring, teleoperation interface, etc. From the clinical point of view, such systems will require the surgeons to review their operating procedures accordingly.

1.2.3. *Intracorporeal mobile devices*

The development of microtechnologies enables designing smaller and smaller low-cost components and integrating them onto multifunction robotized platforms. In this context, the combination of mobility and manipulation is very attractive. This synergy has proven its potential over the last two decades in field robotics. It is thought to be an efficient solution to access and treat targets that are not reachable with conventional surgical approaches.

As of today, attention has mainly focused on actuated colonoscopes and wireless capsules for endoscopy. Capsule endoscopes, passively traversing the GI tract, are now commercially available, as presented in this section. Current research aims at providing them with active locomotion capabilities. Less effort has been made on mobile devices for navigating on the surface of organs, but two examples of such devices will also be presented in this section.

1.2.3.1. *Actuated colonoscopes*

Colonoscopy, and beyond, the exploration of the GI tract, is a procedure that can effectively benefit in the short-term from advances in robotics. It allows the surgeon, among others things, to detect and remove polyps in the colon before they degenerate in cancerous lesions. It consists of introducing through the rectum a colonoscope of 10–15 mm in diameter, made up of a light source, an optical system and service channels (air, water, instruments). The gastroenterologist’s challenge is to push the colonoscope up to the junction of the small intestine (typically 1.5 m from the rectum to the cecum) while controlling the orientation of the head of the instrument using rollers in order to go through colic angles. The colonoscope has a substantial intrinsic stiffness (due to the sheath containing optical fibers and cables for deflecting the head), which allows the doctor to convey the push, but induces a risk of perforation of the wall (one case out of 2000 cases according to Wikipedia). This exam is usually done under general anesthesia in France, under simple sedation in most European countries, without sedation in some Scandinavian countries[12], in which case the action is uncomfortable, even painful for the patient.

To facilitate the guidance movement of the colonoscope and improve the quality of the clinical examination (5–20% of cancerous lesions will not be detected), several solutions are possible such as to guide the colonoscope through a flexible tube introduced previously and which is stiffened once it is positioned[13]. Other solutions are to add active distal mobilities to guide the head of the colonoscope, to integrate sensors to keep it in axial position and thus reduce the pain felt by the patient, to replace the push produced by the doctor through a self-propulsion, etc.

Originally, work in this area aimed at endowing active mobility to the head of conventional endoscopes [NG 00]. The concept has now evolved into a very lightweight architecture with a reduced diameter flexible sheath to bring the fluids, and connect an endoscopic vision system and instruments as shown in the schematic diagram of Figure 1.15(a) (below). Three examples of implementation are shown in Figure 1.15: the EMIL robot [MEN 01] which is able to move independently in the colon by taking the approach of the inchworm (Ø 12 mm, 115 < length < 195 mm). It consists of two anchoring modules (combining suction and mechanical clamping) and a pneumatic bellow acting as an extensor module. It progresses through successive sequences of extension-retraction: anchoring of the rear module, extension, anchoring the head module, retraction. The functional colonoscope of KIST [KIM 03a] is based on the same principle but improves the integration of functions such as vision, a microcamera, a steering device, a biopsy tool and a water injection channel (Ø 24 mm, 137 < length < 269 mm). A more recent prototype, the Air-emit robot [YAN 12], also inspired by inchworm (Ø 27 mm, 270 mm in length) consists of four artificial rubber muscles in series that are sequentially inflated, thus expanding in the radial direction to anchor against the intestine wall though friction. For these three examples, experiments on pigs have highlighted the limits of the locomotion principle and the friction problems caused by the flexible sheath that completely stops the progression of the device before it reaches the cecum.

12 http://www.fmcgastro.org/default.aspx?page=332.
13 http://www.usgimedical.com/endoscopic.html.

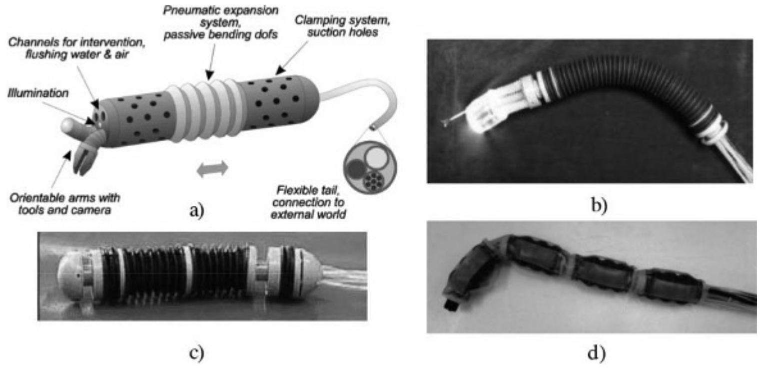

Figure 1.15. *a) Principle of robotized colonoscopy [PEI 01] and different implementations: b) KIST colonoscope [KIM 03a]; c) EMIL [MEN 01]; d) Air-emit [YAN 12]*

1.2.3.2. *Capsule endoscopes*

These capsules are swallowable and progress naturally through peristalsis with the intestinal transit. They have several hours of power autonomy. They are equipped with a light source and one or two minicameras providing images with field of view up to 170° and resolution up to 320 × 320 pixels at 4 Hz. They communicate with the outside world by radio frequency through a transmitter. At least three capsules are currently marketed (Figure 1.16): the ENDOCAPSULE 10 System from Olympus[14] (Japan), MiRO[15] from IntroMedic (South Korea) and PillCam[16] from Given Imaging (Israel). The Sayaka Capsule Endoscopy System from RF System Lab[17] (Japan) is still in development, but we can expect two major improvements such as an inner capsule rotating in a double structure capsule to capture panoramic field of views of the GI, and the absence of a battery, the power being transmitted by a coil through induction. To process the considerable mass of data recorded during an exam (up to 100,000 images), companies provide proprietary software allowing a quick and complete review of the images and providing an aid to the diagnostic.

14 http://www.olympusamerica.com/msg_section/endocapsule/.
15 http://www.intromedic.com/.
16 http://www.givenimaging.com/.
17 http://www.rfsystemlab.com/en/sayaka/index.html.

Figure 1.16. *Examples of capsules (dimensions, number of frames/s (fps), autonomy). From left to right: ENDOCAPSULE 10 System (Ø 11 mm, 26 mm long, 2 fps, 8–12 h); MIRO Cam (Ø 10.8 mm, 24.5 mm long, 3 fps,11 h), Pillcam (Ø 11 mm, 26 mm long, 2 fps, 8–12h), Sayaka (Ø 9 mm, 23 mm long, 30 fps, battery-free)*

The localization of the capsule is still an open issue for these commercial products. A capsule with accurate localization based on magnetic induction was issued by Motilis[18] (an EPFL spin-off company). Yet, the coils in the capsule take all the available space and the capsule can only track its own motion. Nevertheless, it could be very useful for diagnosing abnormal motility (i.e. digestive transit quality), which represents 75% of the troubles in the gut. More recently, Salerno *et al*. [SAL 12] proposed a method for localizing an endoscopic capsule based on an embedded triaxial magnetic sensor that achieves a centimetric accuracy.

Finally, these commercial videocapsules are still passive and need to be turned into real robots, as will be explained later in Chapter 2. The Philips IntelliCap is a good example of an active capsule [SCH 13] that, instead of a camera, embeds pH and temperature sensors to trigger local drug delivery.

1.2.3.3. *Other concepts of mobile robot*

The challenge for these mobile robots is to reach targets on the surface of an organ (e.g. the heart) or within a cavity (e.g. the abdomen) while ensuring adequate adhesion without damaging the tissues. Such robots can then naturally follow the physiological movements of organs that do not have to be stabilized. Both examples presented hereafter are tethered to convey power and motor control, to receive data from biological sensors and camera, and to perform surgical tasks through a service channel.

The *HeartLander* [PAT 05] is an original mobile device developed at Carnegie Mellon University (CMU) for beating-heart intrapericardial intervention. It intends to crawl with an inchworm-like locomotion pattern due to suction pads. Figure 1.17 shows (a) the first prototype and (b) a subsequent version. The front body is attached to three superelastic NiTi

18 http://www.mobilis.com.

wires [OTA 06]: extend, retract and turning phases are accomplished through coordination between the motors controlling the wires and the solenoid valves that regulate the vacuum pressure in each of the suction pads. The total size of both body sections together in the retracted state is 17.7 (length) × 8.2 (width) × 6.5 (height) mm^3. The device has a 1 mm diameter needle channel and a 2 mm diameter general working port.

The *Biopsy robot* from University of Nebraska [REN 06] is driven by differential rotation of two independent wheels designed with helical tread to limit slipperiness (Figure 1.17(c)). The robot is 20 mm in diameter and 100 mm long. A small camera is housed inside the robot between the wheels. The appendage visible in the middle of the cylinder is intended to prevent counter-rotation while allowing the robot to reverse direction. Biopsy forceps are also visible at the end of the appendage. A wireless version of this robot, with an improved design of the inner housing and the wheels, and with improved payload capabilities (an innovative actuated biopsy grasper and physiological sensors) is described in [PLA 08].

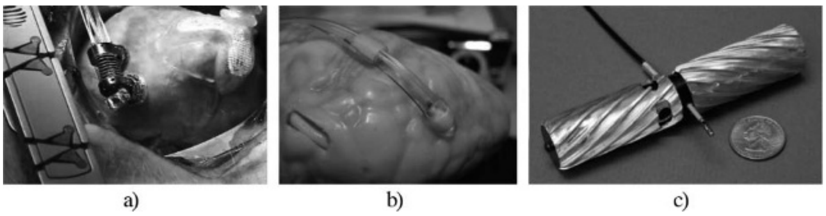

Figure 1.17. *Concepts of mobile manipulators for surgery: a) HeartLander first version [PAT 05] and b) subsequent version [OTA 06]; c) the Biopsy robot [REN 06]*

1.3. Scientific issues

In this section, we address scientific issues that are specific to robotics at milliscale. These issues cover the main fields of robotic research in modeling, design, actuation, sensing and control.

1.3.1. *Modeling*

Modeling for intracorporeal millirobotics may be considered at three levels: robot kinematics, interaction with soft tissues and instrument deformation (as needle during insertion). Kinematic models are necessary for controling the robot while deformation and interaction models may improve the performance and the robustness of a force control scheme.

1.3.1.1. *Modeling of the robot kinematics*

When it is needed for control purposes, usual robotic modeling tools may be used for many devices presented in section 1.2, as their only difference with conventional robots is their size. However, modeling may be an issue for robots with a continuum architecture, such as, for instance, concentric tube robots (see section 1.4.2). It is also an issue for other complex architectures making use of compliant mechanisms such as flexure joints. As reported by Rubbert [RUB 12], these monolithic designs are very promising for surgical applications for several reasons: no backlash and assembly errors, no need of lubricant, no wear debris due to friction, rather simple microfabrication using rapid prototyping techniques, low cost thus disposable or at least sterilizable. However, they require modeling stiffness of the robot links and joints.

1.3.1.2. *Modeling of the environment*

Modeling the environment is necessary to better control the interaction between the instrument and living tissues by improving the stability and robustness of force control schemes. Here, again a trade-off has to be found between real-time constraints, the difficulty of estimating the parameters of the models and precision. On the basis of these criteria, Moreira *et al.* [MOR 12a] only retained the four linear models shown in Figure 1.18 that are composed of a single spring for the elastic model, and serial and/or parallel arrangements of springs and dampers for the viscoelastic models. The corresponding interaction forces are given in Table 1.1.

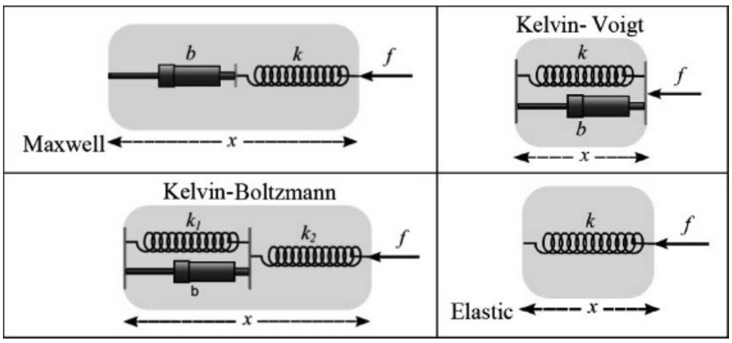

Figure 1.18. *Classical viscoelastic models for real-time uses and purely elastic model*

Model	Equation
Elastic	$f(t) = k\,x(t)$
Kelvin-Voigt	$f(t) = k\,x(t) + b\dfrac{dx(t)}{dt}$
Kelvin-Boltzmann	$f(t) = \beta\,x(t) + \alpha\dfrac{dx(t)}{dt} - \gamma\dfrac{df(t)}{dt}$
Maxwell	$f(t) = k\,x(t) + \alpha\dfrac{df(t)}{dt}$

Table 1.1. *Soft tissues model: f(t), interaction force; x(t), position deformation; k, spring stiffness constant; b, damping factor:* $\alpha = b/k$ *for Maxwell model;* $\alpha = bk_2/(k_1+k_2)$; $\beta = k_1k_2/(k_1+k_2)$; $\gamma = b/(k_1+k_2)$ *for Kelvin–Boltzmann model [MOR 12a]*

Purely elastic models cannot accurately describe interaction between an instrument and soft tissues whose viscous behavior has a strong influence, especially when fast movements are involved. Recall that stress relaxation describes how a material relieves stress under constant strain, and that creep describes how a material strains under constant stress. It comes from the derivative terms of the equations that the Maxwell model is good at predicting stress relaxation but fairly poor at predicting creep. Conversely, the Kelvin–Voigt model is good at predicting creep but fairly poor at predicting stress relaxation. Moreira *et al.* [MOR 12a] have run *in vitro* relaxation tests on a piece of beef. From position input and force output measurements, they estimated the parameters of each models. They showed that the Kelvin–Boltzmann model had the most accurate dynamic and static behavior among the four models and gave the lowest error and lowest root mean square error (Figure 1.19). This can be explained by the presence of both the force and position derivatives in the model.

1.3.1.3. *Modeling of the instrument*

Modeling the robot and the environment may not be sufficient if the instrument held by the robot has non-negligible elastic behavior. This is the case with steerable needles used during percutaneous procedures such as biopsy, drainage of fluids or brachytherapy. Compared with a conventional rigid needle, they can be actively controlled to avoid critical areas by combining insertion and axial rotation (spinning) to change the curvature of the path. Ultimately, a straight path may be achieved by continuously and rapidly rotating the needle as it is inserted. When inserted into soft tissue, Webster III *et al.* [WEB 06b] have shown that a steerable needle follows a curved path that is prescribed by the geometry of its beveled tip (as opposed to a symmetric tip), its relative stiffness with respect to the tissue, and the insertion and rotation velocities at the needle base. They proposed to approximate its kinematic model with that of a non-holonomic unicycle vehicle (as the needle shaft follows the trajectory of the tip, a bicyle model is not required) Figure 1.20(a).

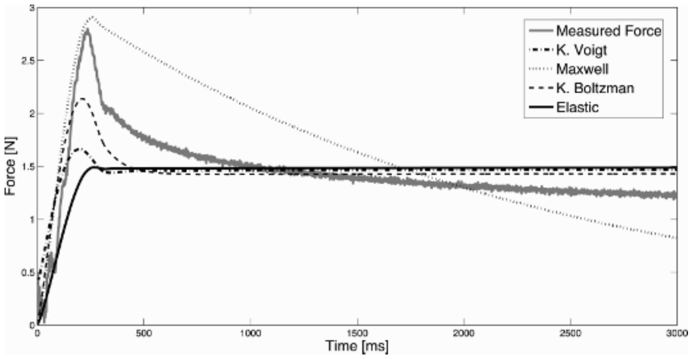

Figure 1.19. *Example of relaxation tests performed on an in vitro specimen [MOR 12a]*

Since this pioneering paper, many works have been done on planning and control of such needles. Minhas *et al.* [MIN 07] introduced the idea of "duty cycled" rotations of the needle to perform insertion with arcs of adjustable curvature. The duty cycle is defined as the ratio of time of rotation to the duty cycle period (time of rotation + insertion). The authors showed that incorporating duty-cycled spinning during needle insertion provides proportional control of the curvature of the needle trajectory through tissue. In a recent work, Bernardes *et al.* [BER 12] proposed to combine closed-loop ultrasonic feedback with an intraoperative, thus online, motion replanning strategy to compensate for system uncertainties and disturbances, and to cope with dynamic changes of obstacles (critical areas) and target positions due, for instance, to physiological motions. Figures 1.20 (b) and (c) give simulation results that confirm the relevance of the method. The work was validated *in vitro* with a six-DoF robot, five DoFs being devoted to the insertion control and one DoF to the duty-cycle control.

Several models have also been developed to estimate the deformation of tissues caused by the insertion of a needle for optimal path planning purposes (see, for instance, [DIM 03, GLO 04, VAN 11]).

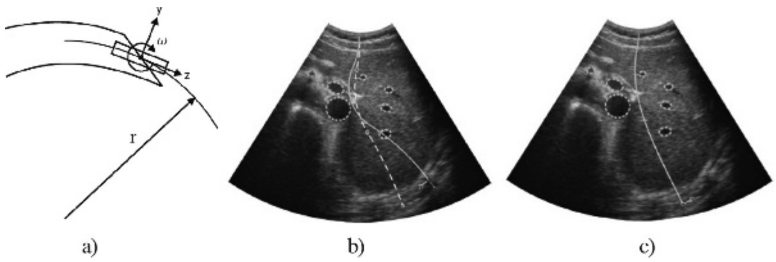

Figure 1.20. *a) Beveled tip needle during steering showing the wheel of the unicycle [WEB 06b]; b) simulated trajectories of the needle tip under disturbances and c) with adaptive replanning for noise compensation: planned path (dashed) and simulated needle trajectory (solid) [BER 12]*

1.3.2. *Design*

The design methodology at a millimetric scale may be the same as described for extracorporeal robots in [DOM 12a]:

− first, is the characterization of gestures and interactions (surgeon/robot, robot/patient, robot/environment) in order to specify the system in terms of the number of DoFs, workspace, speed, effort, precision, etc. Basically, this step requires making use of a force sensor and an optical or magnetic tracking system to collect data for further force and motion analysis;

− then, follows the choice of a kinematic structure and its actuation satisfying the specifications resulting from the characterization step and other constraints such as sterilizability, Computer Tomography (CT) and/or Magnetic Resonance Imaging (MRI) compatibility and safety;

− finally, the synthesis of a controller and the definition of the human machine interface (HMI).

The main difficulties related to the design are:

– the restrictive specifications in terms of power to be transmitted, dimensions and ranges of motion of the instruments;

– miniaturization and integration, including the passage of wires and fluid pipes;

– sterilizability of the device;

– safety, etc.

The diversity of devices presented in section 1.2 shows that conventional kinematics (serial or parallel robots) used in the macroworld cannot cover all the needs within the range of dimensions and forces at millimetric scale. Many other design choices have been explored such as multiarm devices, modular robots, continuum mechanisms, hyper-redundant kinematics, mobile robots, etc. For some applications, such as for GI screening, for instance, bioinspiration is a promising approach to design.[19]

As discussed in [MOG 07], the capsule endoscopes (section 1.2.3.2) suffer from several limitations: among others, they move passively by exploiting peristalsis and they are not able to crawl and inspect a region of interest or to anchor intentionally for a prolonged diagnosis. To give more autonomy to these capsules, several prototypes have been designed, providing them with active locomotion functions mimicking inchworm, beetle, fly, cockroach, fish, etc. Figure 1.21 illustrates some biomimetic locomotion principles (walking, swimming, paddling, etc.) involving legs, cilia, and fins and tails. The inchworm locomotion is certainly the mode that has inspired the majority of solutions. However, as noticed by Menciassi *et al*. [MEN 04], legged locomotion, which is more technically demanding in terms of mechanical hardware and control strategy, has several advantages: faster, no contact or friction with the pathological areas (that could cause ulcers for instance), better adaptation to the luminal diameter, better maneuverability, possible use of legs as a tool, etc. Another benefit is that, due to the leverage effect provided by the legs, the stroke is no longer limited by the length of the body. Finally, legs can be equipped with pads to improve adherence.

Much work has also been done to improve the clamping capabilities of the capsules, especially to avoid mechanical grippers or suction devices that may harm the intestine wall, such as, for instance, the gecko-inspired adhesives developed at the NanoRobotics Lab of CMU[20]. These solutions are alternatives to magnetic guidance that may require a cumbersome external magnetic field generator, as will be presented in Chapter 2.

---

19 As it is for many other non-surgical tasks. For a review, see the issue-focused section on bio-inspired mechatronics, *IEEE/ASME Transactions on Mechatronics*, vol. 18, no. 2, April 2013.

20 http://nanolab.me.cmu.edu/.

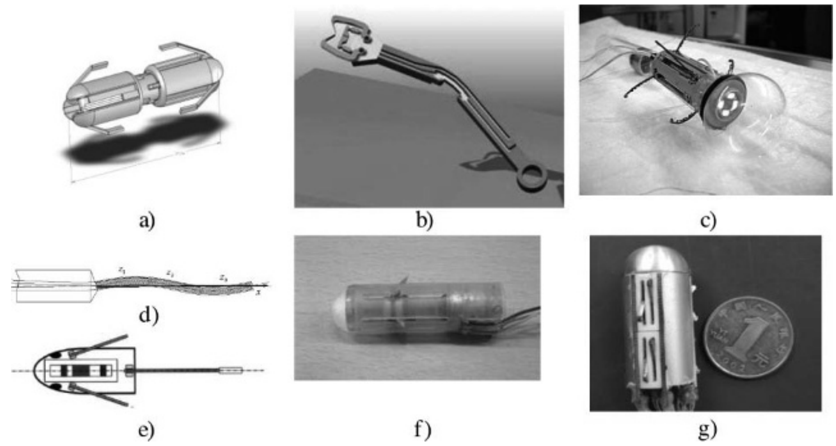

Figure 1.21. *Some examples of biomimetic devices for GI tract inspection: a) inchworm-based locomotion mechanism with legs carrying an adhesive footpad with 4 μm molded PDMS fibers inspired by beetles [CHE 05, KAR 06]; b) bioinspired leg with a compliant knee, including a mechanical grasping system at the tip [MEN 04]; c) legged robotic capsule EMILOC [MOG 07]; d) swimming microrobot with an elastic tail [KÓS 05]; e) swimming robot with fins driven by ICPF actuators (see section 1.3.3) [GUO 02]; f) paddling-based locomotion mechanism [PAR 06]; g) ciliated cell-based locomotion mechanism [LI 06]*

1.3.3. *Actuation and transmission*

The main constraints of the actuators for intracorporeal robotic devices are their biocompatibility and safety, their high output force/torque and, for autonomy, their low power consumption. Many principles of actuation have been explored so far to drive a robot at millimetric scale: conventional principles (electric, hydraulic or pneumatic) such as in the macroworld, and less conventional principles (such as ultrasonic and piezoelectric actuators that are MRI and CT compatible), but also more advanced principles based on active materials. The latter refer to material capable of converting an input energy (electrical, thermal, chemical, etc.) into mechanical work, making it possible to embed the actuation function into the material. The most widely used for intracorporeal robotics are shape memory alloys (SMAs) and electroactive polymers (EAPs). With SMAs, the active principle is a transduction of thermal energy into mechanical energy, while with EAPs it is a transduction of electrical energy into mechanical energy. The most used SMA is NiTi, made up of nickel and titanium, which has an interesting property of biocompatibility. Among the EAPs, two categories are used for the large strain they can produce: the electric polymers that contract under the action of an electric field or Coulomb force, and the ionic polymers such as ionic conducting polymer film (ICPF) that contract under the displacement of ions. EAPs are a promising material for the development of artificial muscles. Additional information on SMA and EAP can be found, for instance, in [PON 05, BAR 04] and in section 2.3.1.1. The advantages and limitations of these principles of actuation in the context of intracorporeal robotics are summarized in Table 1.2.

In Table 1.3, we give some examples of devices (most of them have been presented in section 1.2) to illustrate the various actuation principles. For a more comprehensive review, the reader may refer to [DOM 12b].

Actuation	Advantages	Limitations
Electric actuators	– Easy to control	– Power-to-mass ratio
Piezoelectric actuators	– Low power consumption – High force output – Short response time – Power-to-mass ratio – MRI and CT compatible	– Low strain (0.1–0.2%)→ small stroke – High supply voltage → safety issues
SMA	– Actuation embedded into the mechanical structure – Large strain (up to 8%) – Low cost – Biocompatible (NiTi)	– Slow response time – Heath removal – Relatively low stiffness – Medium output force – High power consumption
EAP	– Low power consumption – Large strain (more than 10%) – Better dynamics than SMA – Low cost – Biocompatible	– Relatively low stiffness – Low output force – Integration issues

Table 1.2. *Comparative advantages and limitations of actuation principles*

Actuation	Examples
Electric actuators embedded in the mechanical structure	DRIMIS [SAL 04], Biopsy robot [REN 06, PLA 08], legged capsule [QUI 07], modular platform [HAR 09], Vanderbilt's dexterous NOTES arms [LEH 08, TIW 10], Araknes [PIC 10, SAN 11], modular platform [HAR 09]
Electric actuators remotely mounted	Hyper finger Mark-3 [IKU 03], HARP [DEG 06, OTA 08], EndoControl JAiMY [ZAH 10], most of the NOTES and SPA devices, Da Vinci EndoWrist, Artisan Extend Control Catheter (Hansen Medical), Amigo RSC (Catheter Robotics)
Piezoelectric	Multi-DoF ultrasonic motor for active endoscope [TAK 01], impact-based piezo actuator [KIM 05], swimming microrobot [KÓS 05], piezoelectric-driven laparoscopic instrument [ROS 09], MICRON handheld instrument for eye surgery [RIV 03], concentric tube continuum robot [SU 12]
Pneumatic	Heartlander [PAT 05] Semi-autonomous colonoscopes: EndoCrawler [NG 00], EMIL [MEN 01], KIST colonoscope [KIM 03a], Air-emit [YAN 12]
Hydraulic	Catheter for microneuroendoscopy of spinal cord (EU FP7 MINOSC project) [ASC 03], microhydraulic active catheters [HAG 05, IKU 06]
Magnetic	*Internal magnetic field:* active capsule endoscope [WAN 06] *External magnetic field:* swimming microrobot [GUO 05], (re)-configuration of swallowable modular robot [NAG 07, NAG 08]
SMA	Earthworm [LEE 04], ciliated capsule [LI 06], legged capsule [KAR 06], catheter [SZE 11], intracranial robot MINIR [HO 12]
EAP	Fish-like underwater microrobot [GUO 02], ciliary motion based walking robot [KIM 03b]

Table 1.3. *A few examples of actuation for intracorporeal millirobots and entry points of related literature*

The actuation principle affects the design of the robot, in particular when electric actuators are remotely mounted. For robots with a limited number of rigid links and discrete joints, the transmission of power may be made, as shown in Figure 1.22:

– by cables (textile or steel) or metal strips: the advantages (compactness, reflectivity of forces in the absence of frictions, etc.) have their counterparts (small radius of the pulleys reducing the reliability of the cables, tricky assembly, etc.);

– or by rigid linkage mechanisms such as pushes and rods: the gain in stiffness is at the expense of the compactness and simplicity of the robot.

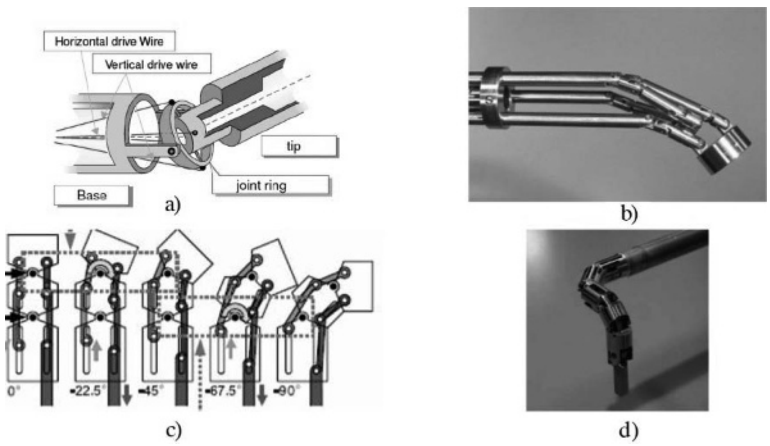

Figure 1.22. *Examples of transmission of power by cables: conceptual design of the "ring joint" of "hyper finger" (see Figure 1.6) driven by decoupled wire-drive mechanism [IKU 03] a); transmission of power by rigid linkage mechanisms: four-DoF parallel kinematic instrument tip for laparoscopy [ROS 09] b); conceptual design c) of a two-DoF bending mechanism of a forceps [YAM 03] d)*

For continuum robots, the design is more complicated and several technological possibilities have been explored. A number of prototypes have been designed based on NiTi super-elastic wires or springs/coils that allow achieving significant angular deflection with a more or less small radius of curvature. A few examples are shown in Figure 1.23, illustrating the design of joint by stacking spheres linked by tendons and the design of flexible joints.

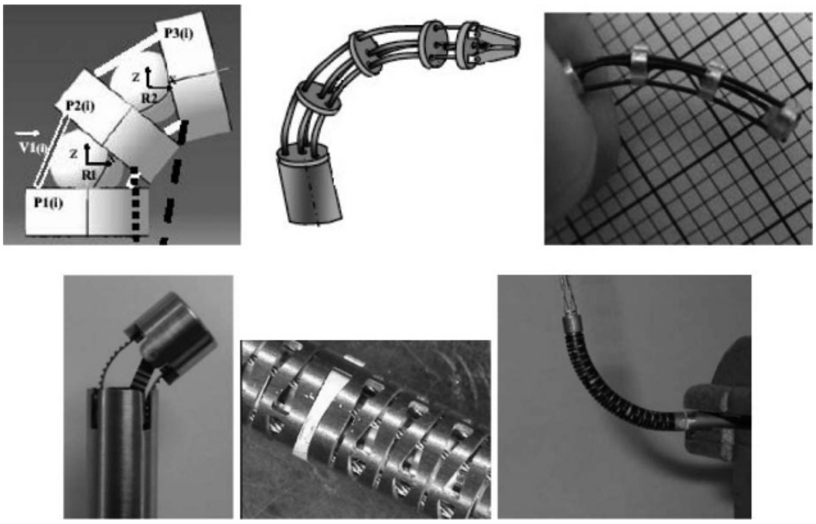

Figure 1.23. *Examples of distributed and flexible joints for continuum robots: above, from left to right: assembly of ball joints and vertebrae to design a forceps holder [VAN 05]; conceptual design and prototype of the "distal dexterity unit" composed of a multibackbone snake-like robot equipped with a parallel tip for throat surgery [SIM 05]. Below from left to right: two-DoF bending manipulator using NiTi spring-link mechanism [ARA 10]; close-up of a machined NiTi spring used in the two-DoF forceps holder (below, right) [PEI 03]*

1.3.4. *Sensing*

At this scale, the same principles are used for vision as in extracorporeal robotics (rigid or flexible full high-definition (HD) endoscopes, which is the current resolution standard for endoscopy, with the slow emergence of on-the-shelf 3D solutions, for instance, from Karl Storz). Force sensing is still an issue, as it is in extracorporeal robotics, and has yet not been widely introduced in the OR. This can be explained by the following stringent specifications:

– From the design point of view, the force sensor has to be small, easy to mount (including the integration of electric wires), biocompatible, sterilizable or disposable (thus low cost) and reliable, all of which raise several difficulties. Typically, the forces may range from a few millinewtons (to detect and manipulate tissues) up to 50 N or more to grip a needle, with a sensitivity of a few tenths of a newton.

– From the operation point of view, the use of a force sensor requires rather complex and time-consuming calibration procedures all over again. The force data have to be properly processed to filter high measurement noise, to compensate for drifts, etc. They also have to be integrated in the control architecture of the robot, which is not possible with most of the on-the-shelf robot controllers.

However, let us recall the importance of force sensing in surgical robotics:

– to measure interaction forces between instrument and tissues for modeling and design specification purposes;

– to feedback interaction forces in a control loop in order to drive the instrument in a comanipulation mode, or to servo the contact force to a desired set point value or to compensate for physiological motions;

– to provide haptic feedback to the surgeon: as pointed out by Menciassi *et al*. [MEN 03] a critical factor in MIS is the severe reduction of sensory capabilities of the surgeon, as finger palpation to characterize tissue hardness or to estimate pulsating flow in vessels;

– to increase safety by stopping the robot whenever excessive forces between the instrument and the tissues are exerted.

During an MIS operation, if the force sensor were mounted at the proximal part of the instrument, it would also measure the forces generated by the friction of the latter due to the passage of the trocar, which can be much greater than the instrument–tissue interaction forces. Thus, different families of solutions have been explored, as summarized in Figure 1.24. The first family consists of integrating miniature sensors at the distal end of the instrument. For example, van Meer *et al.* [VAN 04] designed a sensor based on capacitive detection that was mounted in 5 mm forcep jaws with the possibility to measure forces in two directions (Figure 1.24(a)). The lower example of Figure 1.24(a) [PEI 04] makes use of optical fibers to estimate the deformations of tissues through reflective measurements (Ø 5 mm, range of 2.5 N in axial direction, 1.7 N in radial direction). The second family exploits technologies already developed in the macroworld that are based on mechanical deformation of a beam. A miniature Force/Torque (FT) sensor is placed just before the distal joint (or between the distal joint and the instrument tip) as indicated in Figure 1.24(b). At DLR, Seibold *et al*. [SEI 05] have developed such a six-DoF sensor based on a Stewart platform. Due to its dimension (Ø 10 mm), the ball joints were replaced by flexure joints. For the set of design parameters selected, the load range is Fx,y,z = 30 N, Mx,y = 300 N·mm, Mz = 150 N·mm. The sensor is sterilizable and is now mounted on the DLR MICA instrument (see Figure 1.2) [HAG 10].

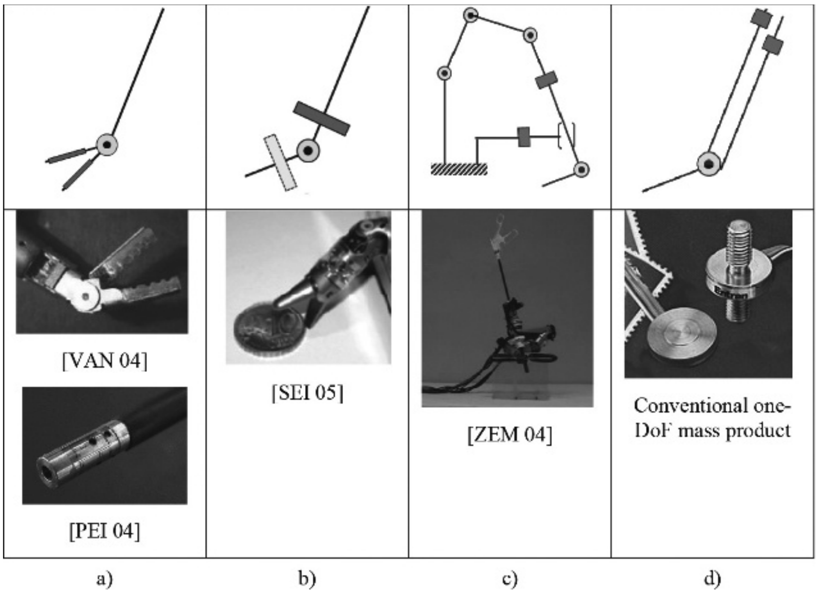

Figure 1.24. *Families of force sensing methods: a) MEMS sensors; b) multiaxis sensor; c) external measurement of interaction forces (MC^{2}E); d) direct measurement of force in the cables when the instrument is cable driven*

The basic idea of the third family shown in Figure 1.24(c) is to make use of two conventional six-axis FT sensors (e.g. from JR3 Inc[21] or ATI Industrial Automation[22]), one mounted at the proximal part of the instrument and the other mounted on the trocar: the advantage of this approach is the reduction of costs and sterilizability constraints. An original implementation of this idea is due to Zemiti *et al.* [ZEM 04] where the instrument is placed inside a passive guidance tube (Figure 1.25(a)). The latter is attached to the upper part of the FT sensor. The lower part of the sensor is placed on a

21 http://www.jr3.com/.
22 http://www.ati-ia.com/.

conventional trocar. If the orientation of the instrument as well as its penetration are controlled by a robot holding the trocar, it is possible to estimate the tool–tissue interaction forces. Writing the generalized forces on the different moving parts, it can be shown that the interaction forces may be easily inferred from the force sensor data if the gravitational forces are known and if the forces due to dynamics are known or negligible. A dedicated device, called MC^2E (a French acronym for compact manipulation for endoscopic surgery) has been designed and validated this approach. It is lightweight and can be mounted directly on the patient. It is a four-DoF actuated mechanism providing an invariant center at the fulcrum point, a frictionless rotation and a translation, respectively, about and along the instrument axis.

The last family of solutions, standing when the distal joints of the instruments are cable driven, consists of directly measuring the cable forces with uniaxial sensors (Figure 1.24(d)). However, the drawbacks (not all the axes are measured, singularities, etc.) are not compensated for by the low cost and rather simple implementation of the sensors in the instrument.

Recently, some other physical principles have received attention. For instance, with a polymer-based touch microsensor glued around the tip of a catheter, it has been shown by Feng *et al*. [FEN 06] that it is possible to feedback to the surgeon small contact forces during intravascular neurosurgery. We already mentioned the work of Peirs *et al.* [PEI 04] estimating the interaction forces from visual information. Such an approach is implemented with the Sensei X system to drive catheter in intravascular procedures. It may require efficient instrument–tissue interaction models and high-performance computational resources to satisfy the real-time constraints of an operation. DiMaio *et al.* have used a 2D linear elastostatic material model, based on finite elements, to derive contact force information during needle insertion, which was processed for graphical and haptic real-time simulation [DIM 03] (Figure 1.25(b)). Basically, this vision-based haptic feedback mimics what the surgeon does in endoscopic surgery. Another approach, based on Moiré fringe, can be used to visually display interaction forces [TAK 10]. The advantage is that it makes use of a cheap and passive mechanism that can be distally mounted on the instrument without requiring embedded electronics and wiring. For a state of the art and an analysis of the problem of force measurement, the reader may refer to [XU 08].

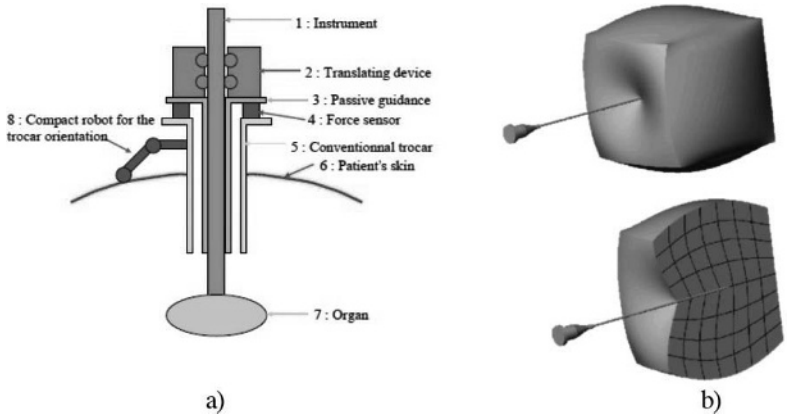

Figure 1.25. *a) Principle of the modified trocar with integrated force sensor allowing for the measurement of interaction forces [ZEM 04]; b) estimation of force during needle insertion from the deformation observed by vision [DIM 03]*

1.3.5. *Control*

As in the macroworld, control may be achieved according to three modes: autonomous, teleoperation and comanipulation modes. However, the latter is much less operable at milliscale and not at all for totally intracorporeal robots. Therefore, the choice of a mode depends on the robot but also on the level of assistance to the surgical gesture that it is intended to provide. This level is specified by the surgeon who is faced, among others, with the problem of sharing authority with a machine, and by the engineer who is faced with conflicting requirements of performance, safety and technological limitations.

1.3.5.1. *Autonomous mode*

What is rather obvious in surgical robotics is that most of the time the surgeon stays in the loop. Except probably for bone machining in orthopedics, most of the tasks are characterized by compliant or semirigid contacts with tissues and cannot be fully automated. However, in many applications autonomous behaviors are required. For the sake of simplicity, we can consider two levels:

– a low level sensory-based control: *force control* [POI 12], for instance, to maintain an instrument against an organ with a desired constant force, such as forceps against a beating heart [ORT 02, DOM 08]; or to virtually increase the stiffness of the robot when it approaches predefined boundaries (also known as virtual fixtures or dynamic/active constraints) as implemented on the Acrobot system [JAK 03]; *visual control* [GAN 12], for instance, to track and maintain an instrument in the field of view of a laparoscope [VOR 07]; or to track 3D motion of organs to compensate for physiological motions [RIC 10];

– a higher decisional level where the robot is supposed to generate a motion and to move autonomously along a path computed from multisensory information, for instance, to reach a target with a steerable needle as in [BER 12] (Figure 1.20(c)).

1.3.5.2. *Teleoperation*

In teleoperation mode, the surgeon acts on a device (the master manipulator or master console) that, in turn, acts through a communication channel on a distant slave manipulator holding the instrument (Figure 1.26). It has been shown that the distance between the master and slave manipulators could be large, which paved the way to tele-echography [VIE 06] and telesurgery [MAR 01] applications where the patient is in a remote or non-accessible location such as a space shuttle or on a battlefield. However, issues such as communication flows and delays, cost of communication networks and safety of connection limit their possible development, mainly for surgery. In most surgical applications, both the master and slave manipulators are much closer, generally in the OR.

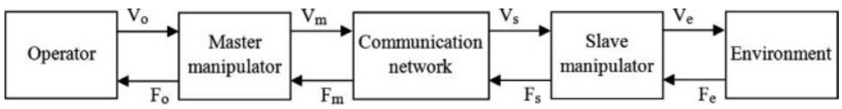

Figure 1.26. *General architecture of a teleoperation system (the symbols V and F denote velocities and forces)*

Many books and articles have been published on teleoperation since the first master–slave system was built by Goertz in the mid-1940s [GOE 54]. A good introduction to the control of these systems can be found in the reference paper of Lawrence [LAW 93] who introduced a generic bilateral teleoperation architecture, which may include up to four channels of data transmission (force and velocity in both directions). The performance of a teleoperation system is assessed by its transparence (ideally meaning that the impedance of the system should be close to zero such that the surgeon does not “feel” its weight, friction or inertia) and its stability (any bounded displacement or force input to the system will result in a bounded displacement or force output). Practically, the control laws of the systems are intended to provide the best trade-off between transparency and stability that are conflicting design goals as shown by Lawrence.

As already mentioned in section 1.2.1, several master–slave architectures have been designed for MIS over the last two decades, among which the first commercial systems ZEUS (Computer Motion) and Da Vinci (Intuitive Surgical), and more recently for research purpose, the platforms Raven II from University of Washington [HAN 13] and MiroSurge from DLR [HAG 10]. We will go into more details about teleoperation architecture in section 1.4.1 with the example of the SPRINT robot of the EU FP7 Araknes project (Figure 1.5). More on teleoperation in surgical robotics may be found in [BAY 12].

1.3.5.3. *Comanipulation*

In comanipulation (also known as hands-on robotics or cooperative robotics), the surgeon holds and manually moves the instrument while the robot follows the resulting motion. Morel *et al.* [MOR 12b] have defined two main categories of systems: the serial comanipulator that adds mobilities in series to the arm of the surgeon (for instance a handheld laparoscopic instrument as JAiMY shown in Figure 1.2), and the parallel comanipulator that can exert forces on the instrument in addition to those produced by the surgeon or maintain it in position when the surgeon no longer holds it. Thus, with a serial comanipulator, the velocities of the surgeon and the active instrument are summed, while with the latter, forces are summed.

As already pointed out, regarding intracorporeal millirobotics, comanipulation may be used only to control partially intracorporeal devices. A significant benefit of such a control is the active filtering of high frequencies to limit the natural tremor of the surgeon. The handheld instrument MICRON from CMU [RIV 03, ANG 04] (Figure 1.27(a)) for vitroretineal applications in eye microsurgery is a good example of serial comanipulator providing active tremor compensation in 3D. It consists of two functional subassemblies: a sensing system (made up of three dual-axis accelerometers plus a triaxial magnetometer, and a data processing unit) that separates the tremor signal of the intentional movement and a three-DoF parallel manipulator with piezoelectric actuators controlled with the tremor signal that stabilizes the position of the tip of the needle. A more detailed description of the MICRON is given in section 1.4.3.

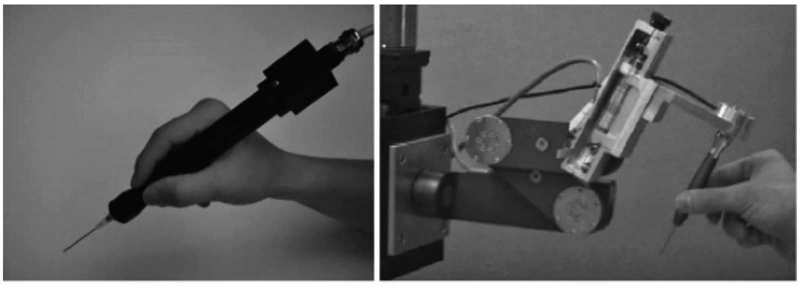

a) b)

Figure 1.27. *Examples of serial and parallel comanipulators: a) the MICRON [ANG 04] and b) the Steady-Hand robot [TAY 99]*

A representative example of parallel comanipulator is the Steady-Hand robot from John Hopkins University designed to perform submillimeter manipulation tasks [TAY 99] (Figure 1.27(b)). As outlined by the designers, the goal of the system was to provide manipulative transparency and immediacy of handheld tools, typically for ENT and eye surgery. The basic idea of the controller is a low-bandwidth force loop. The measured force exerted by the surgeon serves as set point of an inner velocity loop: the low-frequency forces, corresponding to the intended movement, generate a displacement while the high-frequency forces, corresponding to the surgeon's tremor, are blocked.

More on comanipulation in surgical robotics may be found in [MOR 12b]. Table 1.4 summarizes the comparative advantages and limitations of these three modes. An interesting comparison of microsurgery manipulation aids may be found in [MAC 12].

1.4. Examples of devices

We present hereafter a more detailed description of three examples of devices, illustrating different approaches and technologies for intracorporeal surgery at millimetric scale. In the first example – the robotic platform of the Araknes project for SPA surgery – microfabrication techniques such as micro-EDM (electrical discharge machining) were used to design the arms. However, the control techniques are the same as those commonly used for conventional robots in the macroworld. In the second example – a snake-like robot made up of concentric super-elastic tubes – the material and technology used raise new challenges of design and modeling. The last example – the

MICRON handheld instrument – highlights the interest of an integrative approach combining perception, data processing and robotics to develop smart instruments for microsurgery.

Mode	Advantages	Limitations
Autonomous	– Well fitted for complex machining of rigid materials such as bone cutting or milling; or to reach or return to memorized poses – Compensation of physiological motions (beating heart and respiratory movements)	– Description/learning of the surgeon's gesture to the robot – Modeling of the interactions with soft tissues – Safety issues more stringent that with the two other modes (the surgeon is not in the loop)
Teleoperation	– Intuitive manipulation of the instrument through the master interface, discarding the programming/learning phase – Compensation of physiological motions – Filtering of surgeon's tremor – The surgeon may be kept away from possible radiations	– Loss of physical contact between the surgeon and the patient – Cost (master + slave)
Comanipulation	– Best intuitiveness with direct overview of the operating field and direct manipulation of the instrument – Maintaining physical contact between the surgeon and the patient as in MIS – Filtering of surgeon's tremor	– More difficult to compensate for physiological motions – Sharing the workspace between the surgeon and the robot may introduce additional safety and design constraints – The surgeon is exposed to possible radiations – Restricted use for intracorporeal robotics

Table 1.4. *Comparative advantages and limitations of the control modes*

1.4.1. *The robotic platform of the Araknes project* [23]

The objective of the robotic platform of the EU FP7 Araknes project[24] was to transfer the technology of bimanual laparoscopic surgery to scarless single port endoluminal surgery (i.e. moving the required DoFs inside the peritoneal cavity, in which the robots are inserted through an umbilical or esophageal trocar). To assess the interest of such a platform, and to better define both hardware and software specifications, bariatric surgery procedures, aiming at reducing the size of the stomach, were chosen. From the hardware point of view, the robotic platform consists of:

– a dual-arm, SPRINT [PIC 10], already shown in Figure 1.5;

– an HMI based on two modified Omega.7 haptic devices (Force Dimension[25]). The handles were customized and ergonomically designed to reduce fatigue. They are equipped with contact sensors, which allow detecting whether the surgeon is using the HMI, and brakes to freeze the absolute pose of the devices when released by the surgeon;

– an external positioning platform: SPRINT is attached to an umbilical access port that is held and positioned using a double-delta parallel manipulator known as DIONIS (Figure 1.28) [BEI 11]. This dedicated kinematics provides a stiff support and generates a so-called remote center of motion (RCM) at the umbilicus level. It is manually controlled through a joystick to pre-position SPRINT in the area of interest and, at the moment, the motion of this external manipulator is not synchronized with the motion of the dual arm;

– a panoramic camera and an HD 3D camera developed and currently commercialized by Karl Storz GmbH[26];

– various macro- and nanobiological sensors (i.e. Raman spectroscopy, 2D Optical Coherence Tomography (OCT) and tissue ischemia) for diagnosis

---

23 Most materials of this section are from the PhD dissertation of A. Sanchez [SAN 13].

24 http://www.araknes.org/home.html.

25 http://www.forcedimension.com/.

26 https://www.karlstorz.com/cps/rde/xchg/SID-11573738-1ECEC66A/karlstorz-en/hs.xsl/14340.htm.

purposes, such as additional diagnosing tools that complement the information collected by the surgeon when palpating tissue during open surgery[27];

– a surgeon console with a commercial 3D monitor and dedicated chair and desk.

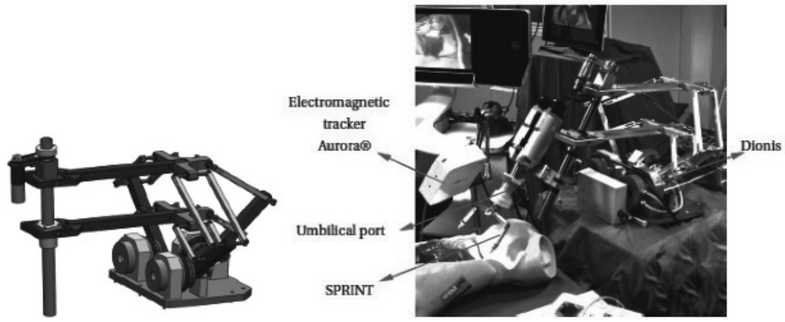

Figure 1.28. *CAD view of the umbilical port holder DIONIS (left) and its integration in the Araknes platform (courtesy of the BioRobotics Institute, SSSA, Pisa, Italy)*

Table 1.5 presents mechanical specifications of the dual-arm SPRINT, which can be compared with the ones of Endowrist from Da Vinci, IREP and DRIMIS. It is worth giving more information and discussing some design choices that have been made for SPRINT:

– The system has a total of 18 DoFs completely located inside the patient's body, i.e. each arm providing six DoFs (plus one DoF for grasping) and DIONIS providing four additional DoFs.

– A serial kinematics was preferred to a parallel one for its large workspace, high dexterity and obstacle avoidance capabilities.

– The actuators are miniature electrical motors (EC series, Maxon Motor AG, Ø 6 mm) that can be sterilized if needed. Custom low-level actuator control electronics that could also be sterilized and embedded in the arm were developed by ST Microelectronics, a partner of the Araknes project.

– Because of the power limitation of the actuators, the maximum force that can exert the tip of an arm is 5 N. This is not enough with respect to the

27 As discussed in section 1.3.4, many R&D efforts have yet to be done to develop force sensors suitable for the OR.

liver retraction task (that may require up to 30 N), which will continue to be achieved by employing a conventional retractor, but is enough to perform the other conventional tasks such as suturing. Furthermore, the gripper is tendon driven allowing gripping forces up to 15 N.

– Given the small size of the arms (Ø 6 mm), the only available sensors are the relative encoders of the miniature motors. Moreover, the impossibility of obtaining measurements at the joint level aggravates the effects of mechanical backlash (up to ±8 mm in the horizontal and vertical planes). Hence, a calibration procedure to compensate for these nonlinearities has had to be set up. To this end, an electromagnetic tracker (Aurora® by NDI Inc.,) was used to register the positions of markers stuck on the base and on the end effector of the SPRINT.

– Given the low dynamic requirements of the tasks and the software-limited operational speeds (for safety reasons), no significant joint (nor link) flexibility issues were observed.

– The platform complies with surgical constraints such as sterilizability, electrical isolation and biocompatibility for temporary contact with body organs lasting 1 h on average.

– The size, principally the diameter, should be reduced in the next version of the prototype.

Parameter	*SPRINT*	*da Vinci* (EndoWrist)	*IREP* [a]	*DRIMIS* [b]
Maximum arm diameter	18 mm	5 mm	6.4 mm	10 mm
Umbilical port diameter	34 mm	N/A[c]	15 mm	N/A[d]
Maximum force	5 N	> 16 N	2 N	< 5 N
Cartesian speed	1 m/s 360°/s	–	0.03 m/s 60°/s	–
Arm length	120 mm	N/A	75 mm	100 mm
Number of internal DoFs	7	4	7	10
Repeatability	±1 mm –	±1.05 mm [e] –	±0.25 mm ±1°	–
Wrist roll range	±∞	±90°	–	±130°
Wrist pitch range	[+130°, −90°]	±90°	–	±90°
Gripper opening	150°	150°	–	–

a[BAJ 12].
b[SAL 04].
cNot applicable, robotic arm outside the peritoneal cavity.
dNot conceived for single-port access surgery.
e[HAI 09].

Table 1.5. *Mechanical specifications of SPRINT compared with EndoWrist, IREP and DRIMIS instruments [SAN 13a]*

Regarding the real-time control architecture [SAN 11], Table 1.6 summarizes the general hardware and software specifications. It is important to take into account that during the control of a surgical robot, if control tasks miss a deadline, a threat to the life of the patient could exist. Thus, a hard real-time operating system (RTOS) is mandatory in order to ensure that the system operates in a deterministic manner. In general, the developed software of the control architecture is based on open source components. Nowadays, these solutions are highly portable and customizable, which are desirable features in order to reuse such a system in future medical robotics projects.

Parameter	Description
RTOS	Hard real-time with Linux RTAI
High-level control frequency	1 kHz
Low-level control frequency	10 kHz
Communications with low-level controller	Ethernet MTAP protocol
Communications with surgeon's console	Ethernet UDP protocol
Programming language	mainly C, some C++
Documenting tools	with Doxygen v.1.8.2
Version control	Subversion v.1.7.7
IDE	Eclipse
No. of processors	3 @ 2.8 GHz (Dell Precision 650)

Table 1.6. *Control architecture specifications summary of the Araknes platform [SAN 13a]*

In addition, real-time communications between the high- and low-level actuator controllers are guaranteed by using a proprietary protocol developed by ST Microelectronics – Multimaster Tokened Access Protocol (MTAP) [CAL 08] – which allows to achieving a high-level control frequency of 1 kHz. At low level, the electronic boards developed by ST Microelectronics provide pulse width-modulated voltage regulation for the actuators. In the current implementation, this voltage regulation is performed using a closed-loop frequency of 10 kHz.

Regarding the haptic interface [SAN 12b], a frequency of 1 kHz is also used. This frequency is commonly employed in such devices due to the low human arm bandwidth, and also since such sampling frequency is sufficient to avoid perceiving undesired vibrations of the device. In general, it is very important that the mechanical design does not have resonance frequencies situated within this range. Fortunately, commercially available haptic devices do meet such requirements.

A teleoperation control architecture has been developed. Two teleoperation schemes based on different robot control strategies, i.e. position–position and force–force, have been evaluated in terms of stability and transparency. An active observer was implemented in both cases in order to cope with modeling errors and disturbances. A realistic soft tissue model has also been used for obtaining better real-time approximations of the interaction forces. Figure 1.29 illustrates the master and slave position and force tracking profiles in free space as well as during contact motion for the Kelvin–Boltzmann model (section 1.3.1.2). It should be stated that the movements (Figure 1.29(a)) of the master during the first few seconds do not represent oscillations; rather, they are intentionally created by the operator to assess the system stability and performance in free space. From 40 s to 80 s and 100 s to 130 s, the slave robot is, respectively, in contact with a piece of meat and a so-called Phantom object (a more rigid environment). The results indicate good position matching at the master and the slave sides, showing high performance of the proposed control schemes. Between these two contact tests (from 80 s to 100 s), the operator stopped using the system in order to change the objects.

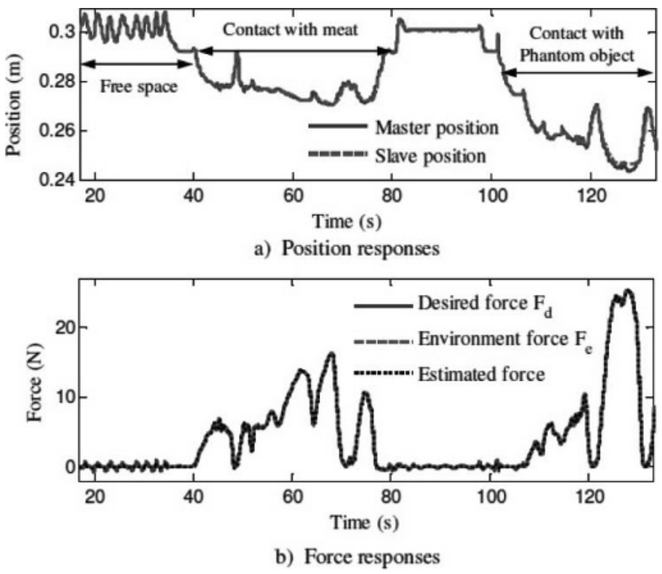

Figure 1.29. *Tracking performance of the teleoperation based on a K-B model of interaction [SAN 12a]*

Figure 1.29(b) shows the corresponding force including the desired force, the interaction force with the environment, and the estimated force in free space and under contact motion. Good force tracking performance is achieved during interaction. When the slave makes contact with a piece of flesh, the contact force magnitude is lower than in the case with the Phantom object. Indeed, during interaction with a more rigid object, the operator feels higher force feedback and as a result, he/she pushes against the environment through the master handle, leading to higher level of contact forces.

1.4.2. *A snake-like robot made of concentric super-elastic tubes*

Works on concentric super-elastic tubes for surgery were first presented in 2006 by Sears and Dupont at Boston University [SEA 06] and Webster III at Johns Hopkins University [WEB 06a] (Figure 1.8). They were motivated by the observation of several shortcomings when inserting flexible needles: as noted in [SEA 06], high-curvature steering requires a very flexible needle that leads to problems of buckling as well as excessive torsional flexibility, which can also lead to loss of steering control. Classified in the family of snake-like or continuum robots that can deform continuously, the concentric tubes robots (CTRs), also known as active cannulas, are an alternative to the cable/tendon-driven robots. Their basic features are the following:

– made up of NiTi hollow tubes, thus having super-elastic properties;

– the tubes are pre-bent and inserted inside each other;

– the outer diameter of a tube typically ranges from 0.5 to 2 mm: the smaller the outer diameter, the smaller the possible radius of curvature of the pre-bent tube, allowing it to negotiate tighter turns. However, pre-bending cannot exceed a limit, beyond which plastic deformation will appear;

– a pair of tubes provides two independent DoFs associated with relative translation and relative rotation of the tubes with respect to one another;

– depending on their bending stiffnesses, the behavior of a pair of tubes is different (Figure 1.30) [SEA 06]: when the stiffness of one tube is much larger than that of the other, the concentric tube pair conforms to the curvature of the stiffer tube but the more flexible tube relaxes to its original curvature when translated; when the stiffnesses are similar, the unstressed curvatures interact to determine their combined curvature, leading the curvature to vary when rotating the tubes. These behaviors are defined as a *domination-stiffness* tube pair (with fixed curvature) and a *balanced-stiffness* tube pair (with variable curvature), respectively;

– CTR may combine various sequences of dominating-stiffness and balanced-stiffness tube pairs. Whatever the combination, the common axis of a CTR conforms to the mutual resultant curvature of the constituent pre-bent tubes;

– the lumen of the tubes can house wires for controlling articulated distal instruments, or be used to pass liquid or forms of energy;

– the tubes are individually actuated at their bases by dedicated actuation units that can apply differential rotations or translations. It should be noted that these units are generally bulky, the bulk of the whole controller increasing with the number of DoFs. As they must be close to the patient to limit the length of the tubes, hence the potentially undesired elastic deformations due to excessive length, the setting up of the robot within the operative area may be tricky.

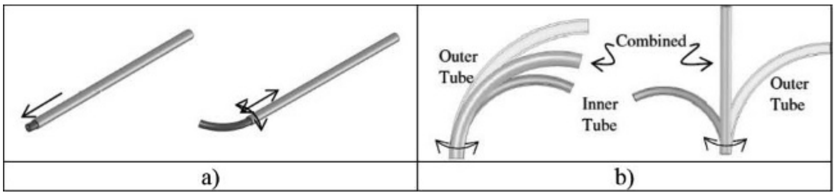

Figure 1.30. *a) Dominating-stiffness tube pair and b) balanced-stiffness pair [SEA 06]*

With such a design, instruments can generate their own steering forces rather than relying on tissue reaction forces [SEA 06]. There are several promising applications requiring high dexterity that rely on the possibility of miniaturization and customization, and on the intrinsically lightweight, modularity and low cost of the technology. Apart from needle insertion procedures, CTRs are well suited for accessing safely deep internal structures: for instance, in [BUT 12], a CTR is used to manipulate a flexible neuroendoscope in brain surgery; in [BED 11], a CTR is optimally designed for intracardiac beating-heart surgery under fluoroscopic and ultrasound imaging; in [SU 12], a feasibility study of a MRI-guided CTR is made for neurosurgery and percutaneous interventions; in [ANO 11], a systematic approach to optimizing the design of CTR for neurosurgical procedures is reported with simulation study results.

Dupont *et al.* [DUP 10] gave design guidelines for CTR. The curvature of individual tubes should be limited to avoid permanent deformation of the robot, and to prevent instabilities due to elastic interactions between torsion and bending of tubes. To manipulate distal links independently of proximal links, and to provide a good dexterity while minimizing lateral forces on tissue, they suggest designing a CTR as shown in Figure 1.31. In this example, the architecture consists of a sequence of five tubes within three telescoping sections of variable, fixed and variable curvature, respectively. The stiffnesses of the tubes are such that each telescoping section dominates all those sections extending from it, hence providing decoupling between links. Furthermore, choosing larger curvatures for the distal sections makes it possible to some extent to decouple tip displacement and tip orientation, as in conventional anthropomorphic robots whose wrists have intersecting axes. In [BED 11], further work has been done to include in the design rules the constraints imposed by a specific task and anatomical environment.

The shape and length of a CTR can be varied by controlling relative translations and rotations of the tubes. This requires deriving a kinematic model, whose complexity should not affect the real-time performance and precision of the position control. Several modeling approaches have been developed. In [WEB 09], the authors made use of minimum energy principles and Lie group theory as a framework for modeling. The starting hypothesis was that the overall CTR shape locally minimizes stored elastic energy. They validated the importance of modeling torsional effects to accurately predict the CTR shape (Figure 1.32). In [DUP 10], a framework for modeling was proposed. It is based on 3D beam-bending mechanics and includes torsion along the entire lengths of the tubes. It is also able to predict the above-mentioned torsion-bending instabilities. However, several effects were neglected such as shear of the cross-section, axial elongation, nonlinear constitutive behavior, friction between the tubes, etc. In [LYO 10], the control of the shape of the CTR was formulated as a planning problem: given the target location, the current CTR configuration, a geometric representation of obstacles and a simplified model that neglects beam mechanics, an optimization algorithm computes the length and orientation of each tube.

As for traditional serial robots, the inverse kinematics of CTR is not straightforward. The challenge is due to the nonlinear mapping between relative tube displacements and tip configuration as well as due to the multiplicity of solutions. A closed-form geometric approach is given for single and multiple sections in [NEP 09] by applying an analytical process to solve inverse kinematics based on modeling of each section with a spherical joint and a straight rigid link. Jacobian-based methods represent another approach to robot-independent inverse kinematics. It finds a single solution to the problem by servoing a virtual copy of the robot from any initial guess (including the robot's current configuration) to the desired configuration (e.g. [SEA 07, WEB 08] for active cannula results). In the Jacobian-based inverse kinematics strategy, it is possible to build actuator limits into the control law so that the robot trajectory is always physically realizable [WEB 10].

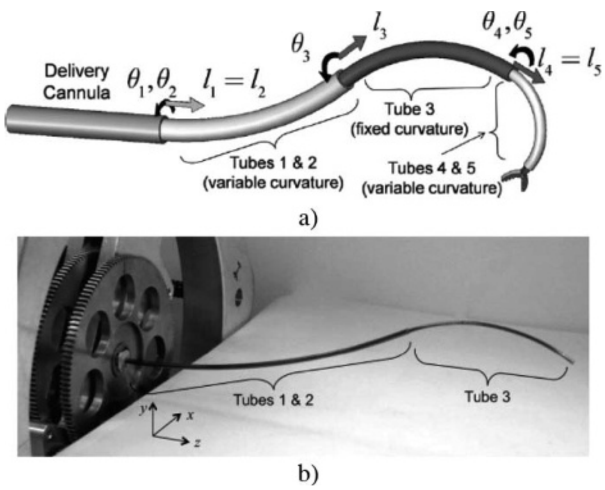

Figure 1.31. *a) Principle of a five-DoF CTR consisting of a sequence of balanced and dominating tube pairs; b) prototype of a three-DoF CTR based on this principle [DUP 10]*

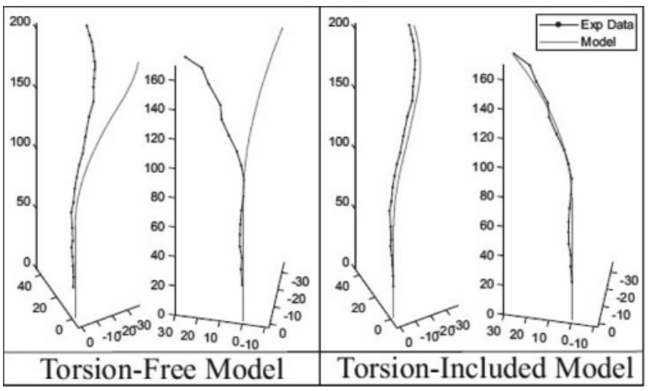

Figure 1.32. *Effect of including torsion in the kinematic model on the shape accuracy [WEB 08]*

Deformation caused by external contact force is another important issue for CTR. It is shown in [LOC 10] that tip loading could increase the mean tip error by almost 50% compared with the unloaded model. In [RUC 10], Cosserat-rod theory is applied to model forward kinematics to describe large deflections as a result of external point or distributed wrench loads.

It can be observed that the identification of robot-dependant kinematics and dynamics properties is essential in developing accurate and realistic CTR control algorithms. Systematic identification and calibration procedures have rarely been reported in the literature and it is expected that further research efforts toward this end would remarkably improve the CTR control performance and benefit newcomers in this area. Also, the use of exteroceptive sensing (namely medical imaging) in the feedback loop could compensate for the CTR model errors and disturbances.

1.4.3. *MICRON: a handheld robotized instrument for ophthalmic surgery*

In ophtalmic surgery, a high degree of precision and dexterity is demanded of the surgeon who has to manipulate very small structures (typically a few tens of micrometers, e.g. for membrane peeling during a vitreoretinal procedure, not exceeding contact forces of a few millinewtons). A further difficulty is the involuntary hand motion of the surgeon that may be one order of magnitude higher (>100 µm RMS in each principal axis) due to the so-called physiological tremor, a quasi-periodic motion (bandwidth between 8 and 12 Hz, >50 µm RMS in each principal axis), to which low-frequency drift and aperiodic sudden jerk components may be superimposed (Figure 1.33, top left). Therefore, it makes sense to investigate the potentialities offered by robots to compensate for these involuntary motions. A few prototypes have been developed since the very beginning of medical robotics, taking advantage of two specificities of the surgical field: (1) the surgeon can directly view the interior of the eye using a microscope; (2) the intraocular targets are close to the outer part of the eyeball, making them rather readily accessible by an instrument. Among the prototypes, let us mention (refer to [MAC 12] for a more comprehensive survey):

– a six-DoF slave parallel micromanipulator from Northwestern University for the treatment of retinal venous occlusion providing microscale spherical movement [GRA 93];

– the ophthalmic microsurgical robot from MIT [HUN 95] and robot-assisted microsurgery (RAMS) from JPL-NASA for vitreoretinal surgery [DAS 99], which are the first master–slave architectures with force feedback designed and used to scale down the hand motion and filter the surgeon's tremor;

– the already mentioned Steady-Hand robot from JHU, USA, for microsurgery, namely ophthalmic surgery (Figure 1.27(b)) [TAY 99]. Unlike the earlier prototypes that are teleoperated, the Steady-Hand is comanipulated;

– more recently, the microsurgical manipulator from Columbia University providing intraocular dexterity [WEI 07b]: it consists of two identical arms attached to a head ring. Each arm is composed of a two-DoF intraocular dexterity robot (IODR) and a six-DoF parallel robot for precise positioning of the eye and the IODR. The IODR is made up of a mobile preshaped NiTi tube inserted in a straight tube that provides a combined translation and rotation motion of the surgical tool as presented in section 1.4.2.

Another approach to ophthalmic surgery is the handheld robotized instrument whose advantages are manifold: intuitiveness, safety, limited intrusion into the surgeon's workspace and low cost. Pioneering work in this area was done by Riviere at CMU , USA, [RIV 03] in the late 1990s with the MICRON (Figure 1.27(a)). The instrument detects its own motion, as does a handheld camera to stabilize the optical image, but it can also distinguish between desired and involuntary undesired motion. Then, the tip is moved in an equal but opposite direction to the undesired motion, the goal being to achieve a positioning accuracy of 10 µm. To meet these requirements, the instrument must perform three functions: motion sensing, estimation of involuntary hand motion and tip deflection control for compensation [RIV 03].

Motion sensing system: this is made up of three dual-axis miniature microelectromechanical systems (MEMS) accelerometers and a triaxial magnetometer housed in two locations as shown in Figure 1.33 (right). The choice of internally as opposed to externally referenced sensors was motivated by the better RMS sensing accuracy (~ 1 µm for an inertial sensor versus ~ 0.1 mm at about 2 m for an optical tracking system), and by the fact that it does not require maintaining a line of sight with an external reference source. Furthermore, an all-accelerometer solution compared with a conventional inertial navigation system with miniature gyros, offering the same quality in linear and angular inertial sensing, is justified by the poor resolution of the latter. The signals delivered by the sensors are then processed to compensate for deterministic errors and properly fused to derive the position and orientation of the instrument.

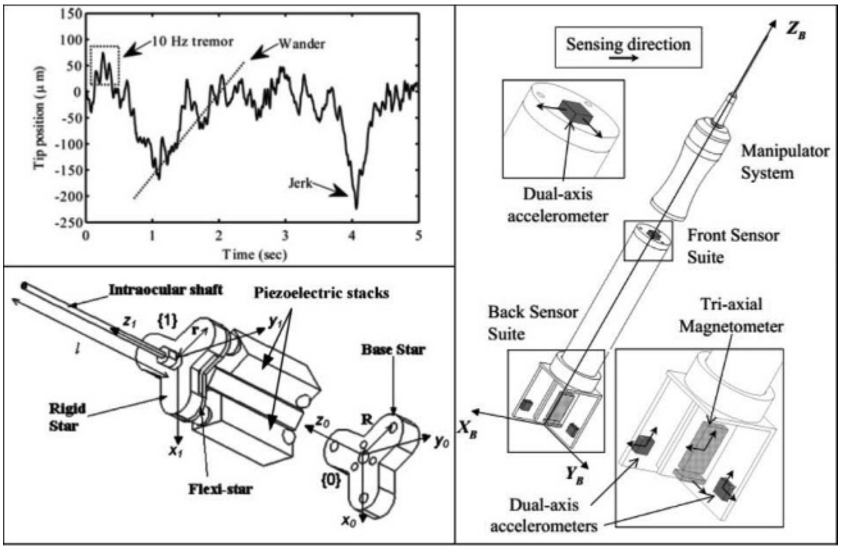

Figure 1.33. *Tremor signal and non-tremulous errors (top left) [MAC 12]; kinematics of the parallel manipulator (bottom left) [ANG 04]; sensing system design (right) [ANG 04]*

Estimation of involuntary hand motion: as mentioned above, tremor has an 8–12 Hz bandwidth, which is higher than the one of a voluntary motion (<1 Hz). However, a simple low-pass filter would cause a phase change between the input and output signals, hence a time delay lessening the positioning accuracy. In the approach proposed by Riviere *et al*. [RIV 03] and Ang [ANG 04], tremor is modeled as a quasi-periodic signal of unknown frequency within this frequency band. A weighted-frequency Fourier linear combiner (WFLC) is applied to the input signal after a band-pass filtering process to eliminate voluntary motion (below 7 Hz) and noise (>13 Hz). The resulting estimation of the tremor frequency is fed to a Fourier linear combiner (FLC) algorithm that adapts online the reconstructed tremor signal to its time-varying reference frequency online.

Tip deflection control: Figure 1.33 (bottom left) illustrates the principle of the three-DoF parallel singularity-free manipulator that has been designed to actively control the instrument tip. Referring to [RIV 03], the plastic "flexi-star" constrains the manipulator against rotation about the longitudinal axis and translation in directions transverse to this axis. Its center is clamped to the stationary center column of the instrument, and the tip of each leg is pinned to the corresponding leg of the rigid star that holds the intraocular tool shaft. Each actuator consists of seven piezoelectric stacks, with the last stack resting against the base star. The choice of piezoelectric actuators is justified by their compactness in size (each stack measures 5 mm × 5 mm × 18 mm), high actuation force (840 N), large operating bandwidth and rapid response time (<50 µs). In return, the presence of hysteresis can attain 15% of maximum displacement. The maximum transverse and axial tip displacements with such a design are, respectively, 650 µm and 100 µm. From the control point of view, as the position of the tip is not measured, an open-loop strategy was implemented: given the estimated tremor signal as input, an inverse kinematics algorithm computes the joint variables of the parallel manipulator; then, an open-loop feed-forward controller with an inverse hysteresis model generates the reference signal to drive the piezoelectric actuators.

Figure 1.34 illustrates the performance of a MICRON of the first generation. Several subsequent versions have been developed since then [MAC 12] to improve performance (namely by active compensation of low-frequency and aperiodic motion; by reducing errors due to hysteresis by an appropriate control of the total charge stored in the actuator rather than the applied voltage; and by reducing backlashes due to the use of flexure joints) and to circumvent shortcomings (reduce size, provide greater range of motion and higher bandwidth).

Figure 1.35 shows a more recent version of the MICRON: it has a 400 µm range of motion at the tip of a typical 40 mm tool, 1 N force capability and a bandwidth more than 100 Hz; the inertial sensors that do not accurately detect the lower frequency components of hand motion (well below 10 Hz) were replaced by a system of two dc-optical sensors (position-sensitive detectors (PSDs)) that track three infrared LEDs mounted on the tool-holder and one LED on the handle allowing closed-loop control (with a resolution of 4 µm at a rate of 2 kHz). Figure 1.35(a) shows a “descendant” of the MICRON, the ITrem from Nanyang Technological University (NTU), Singapore [LAT 09] featuring an all-accelerometer inertial measurement unit comprising three optimally placed dual-axis miniature MEMS accelerometers. It also makes use of flexure joints. To compare with the performance of the first generation of handheld instruments, the performance of ITrem is also shown in Figure 1.34.

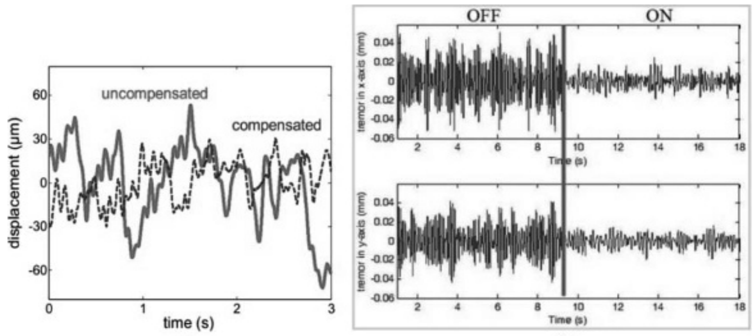

a) b)

Figure 1.34. *a) Performance of the MICRON*[28]*: total range 52% reduction, RMS amplitude 47% reduction (compensated displacement in dashed line, uncompensated displacement in solid line); b) performance of the ITrem*[29]

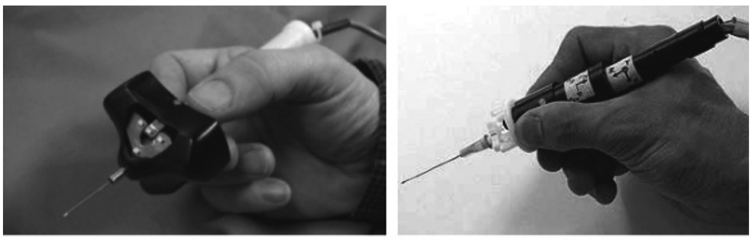

a) b)

Figure 1.35. *a) Last version of the Micron showing tool and position sensor LEDs (max Ø of the LEDs housing=50 mm) [MAC 12]; b) the ITrem from NTU [LAT 09]*

1.5. Conclusion

We have presented in this chapter many prototypes that clearly contributed in some way to the progress of surgical robotics toward the use of miniature and smart robots and robotized instruments in the OR. The variety of applications for which these prototypes have been designed demonstrates the importance of most of the surgical specialties in such progress. For the sake of clarity, we have distinguished three classes of devices providing partially intracorporeal mobilities, then fully intracorporeal manipulation

28 http://www.lirmm.fr/uee05/presentations/lecturers/Ang.pdf.

29 http://www.mae.ntu.edu.sg/AboutMAE/Divisions/RRC_BioRobotics/Pages/IntelligentHandheld.aspx.

capabilities and finally intracorporeal mobility capabilities. The analysis of both functional and technical qualities and limitations of these examples has allowed us to review the scientific issues that are specific to robotics at milliscale, namely in the fields of modeling, design, actuation, sensing and control. Finally, we have described three robotic systems illustrating different scientific and technical approaches for intracorporeal surgery at millimetric scale.

Even if many advances have been made in the last decade, several challenges remain open to expand these systems with functions providing more dexterity in manipulation, more autonomy in movement control and more perception capabilities. Moreover, compared with conventional robots in the macroworld, and aside from miniaturization issues, new difficulties are raised to integrate robotic components and functions at this scale in a compact, robust and safe manner. This justifies in a sense the recent efforts made to radically explore different surgical and technical methods as will be explained in the following chapters.